NOTE TO USERS

This reproduction is the best copy available.

University of Alberta

MATHEMATICAL MODELING OF THERMAL CONVERSION OF ATHABASCA BITUMEN

by

Kevin Chan 

A thesis submitted to the Faculty of Graduate Studies and Research
in partial fulfillment of the requirements for the degree of

Master of Science

in

Chemical Engineering

Department of Chemical and Materials Engineering

Edmonton, Alberta
Spring 2007

Your file Votre référence
ISBN: 978-0-494-45790-0
Our file Notre référence
ISBN: 978-0-494-45790-0

Abstract

The thermal cracking of Athabasca bitumen was studied in a soaker visbreaker. Nine visbreaking runs were performed at five different temperatures ranging from 390°C to 430°C, flow rates of 2 and 3 kg/h, and residence times of 20 and 30 minutes. A new concept was introduced and used to develop a new form of visbreaking model: a method of defining pseudo-components that utilized chemistry information about the feedstock from carbon type analysis. Nuclear Magnetic Resonance (NMR) spectroscopy was used to quantify carbon types found in the pseudo-components in both the feed and products. These data allowed the major chemical pathways followed during thermal conversion to be monitored. Overall, the model consists of two major parts: reaction chemistry pathways describing the formation of light end products and the use of severity index to predict product yields and distributions. Unlike previous visbreaking models, no kinetic parameters needed to be estimated.

Acknowledgements

I would like to thank my supervisors, Dr. Carolina Diaz-Goano and Dr. Heather Dettman, for their support and wisdom throughout my graduate school years. I would also like to express my gratitude to my parents. This accomplishment would not have been possible without their love, support, and guidance throughout my life.

I would especially like to extend my gratitude to my fellow students of Circle K International at the University of Alberta.

The research was supported by the Natural Sciences and Engineering Research Council (NSERC), the Department of Chemical and Materials Engineering at the University of Alberta, the National Centre for Upgrading Technology (NCUT) through partial funding by the Canadian Program for Energy Research and Development (PERD), the Alberta Research Council and the Alberta Energy Research Institute. As well, the researchers wish to acknowledge Dr. San Yip, Dr. Theo de Bruijn and the NCUT Highhead Group for performing the visbreaker runs, Ms. Sara Salmon for analysis coordination and quality control, Ms. Anna Truong for preparing the SARA fractions, and the NCUT Analytical Group for performing the distillations and analyses.

Table of Contents

List of Tables

List of Figures

List of Symbols

τ	Reactor Residence Time
2ET	2-Ethyltetralin
A_o	Arrhenius Pre-Exponential Factor
BP	Boiling Point
DDP	1-Dodecylpyrene
E_A	Activation Energy
ERT	Equivalent Residence Time
G	Gas
GLN	Gasoline
GO-A+P	Gas Oil Aromatics+Polars Pseudo-component
GO-S	Gas Oil Saturates Pseudo-component
k	Reaction Rate Constant
LGO	Light Gas Oil
N	Naphtha Pseudo-component
NMR	Nuclear Magnetic Resonance
PDB	n-Pentadecylbenzene
R	Universal Gas Constant
R-A+P	Residue Aromatics+Polars Pseudo-component
R-As	Residue Asphaltenes Pseudo-component
R-S	Residue Saturates Pseudo-component

SARA Saturates, Aromatics, Resins, Asphaltenes

SI Severity Index

T Temperature

TDC n-Tridecylcyclohexane

UDD 1-Undecyldecalin

UDN 1-Undecylnaphthalene

VGO Vacuum Gas Oil

X Conversion

Chapter 1

Introduction

Petroleum refineries aim to maximize production of products such as transportation fuels and minimize the waste of their petroleum feedstock. The transportation fuel products are gasoline (boiling point (BP) < 170°C), jet fuel (BP: 170-270°C), and diesel (BP: 250-380°C) [1]. These fuels are light end products and are small molecules. Petroleum feedstocks have considerable contents of material that have boiling points above 380°C. The large molecules in the 380°C+ fraction need to be cracked to transform the big molecules into smaller molecules and produce the light end products. Catalytic cracking is often not useful for cracking heavier fractions because the high nitrogen, sulfur, and metals content of heavy fractions tend to poison the catalyst. Another alternative for processing is thermal cracking.

1.1 Modeling of Thermal Cracking Processes

As heavier feedstocks are being used more around the world to meet the growing demand for energy, the need to understand the thermal cracking processes that are used to upgrade these feeds becomes more important. To achieve this, mathematical and kinetic models are developed to help understand thermal cracking processes and thermal chemistry. Modeling also enables the prediction of product yields as well. There are several thermal cracking processes such as viscosity

breaking, residue hydrocracking and coking being used today commercially. For this study, viscosity breaking was chosen because it is the simplest and least severe of the thermal cracking processes.

1.1.1 Challenge for Modeling

One of the challenges of modeling a thermal cracking process is the oil itself. Unlike mixtures of defined components, oil is a mixture with a very large number of real components. Thus, an exact composition is not known. This is especially true with heavy oils and bitumen. The composition of heavy oils is much more source dependent than that of conventional oils. Conventional oils generally have a low content of vacuum residue fraction (BP > 524°C). Lighter oils (BP < 524°C) are more easily characterized by gas chromatography techniques. Heavy oils and bitumen usually have a high content of the vacuum residue fraction. Having a larger content of larger molecules causes more variability in the makeup of the oil because each molecule is different, yet they are not easily characterized.

A comparison of the typical properties of some light and heavy crudes is shown in Table 1.1.

Table 1.1: Comparison of the Properties of Light and Heavy Crudes

	Saladin [2]	Heavy Arabian [3]	Athabasca Bitumen [4]
SG	0.79	0.98	1.01
Sulfur wt%	0.02	4.23	4.9
Nitrogen wt%	<0.01	0.26	0.5
Metals (ppmw)	<5	115	280
+524°C Fraction	<2 wt%	51 wt%	52 vol%

As shown in Table 1.1, the Heavy Arabian crude and Athabasca bitumen have a higher specific gravity (SG) and residue fraction (BP > 524°C) content than the light crude oil. These examples show that the heavier feedstocks have the higher nitrogen, sulfur, and metals contents that are problematic for catalysts.

1.2 Research Objectives

Previously, the development of visbreaking models has focused on estimating kinetic parameters to predict product yields. Thermal cracking chemistry has not been given as much attention during model development. The primary goal of this research is to develop a model to better understand thermal cracking processes and thermal chemistry. In particular, the pathways describing the light end products (gas and naphtha) will be proposed. The model will also be used to predict the product yields and composition from the visbreaking of Athabasca bitumen.

1.3 Thesis Overview

The remainder of the thesis is organized as follows:

- Chapter 2 presents technical background information and proposes the method for model development.
- Chapter 3 describes the experimental methods and the experimental conditions. The steps for fraction preparation and characterization are given.
- Chapter 4 describes the results of the feed and product characterization. The results of elemental analysis, distillation, pseudo-component fractionation, toluene insolubles, and product gas analysis are presented.
- Chapter 5 describes the development of the visbreaking model and the discusses the two parts that make up the model.
- Chapter 6 discusses the steps taken to validate the model and the error analysis. A procedure on how to predict product yields and a discussion of the model are also presented.
- Chapter 7 discusses the conclusions of this study and possible future work.

Chapter 2

Technical Background

This chapter presents an introduction and review of technical background information taken from the literature. Also, new concepts used for model development are introduced and discussed.

2.1 Visbreaking Past and Present

Viscosity breaking, or visbreaking for short, is a process that has been used for many decades to process fractions that have some but not a lot of vacuum residue. Visbreaking is primarily intended to cause a reduction in the viscosity of the feedstock while providing some conversion to light end products. Originally, visbreaking was applied only to atmospheric (BP $>$ 343^{o}C) or vacuum (BP $>$ 524^{o}C) residue fractions. The goal was to reduce the viscosity of the residues enough so that they could be used as fuel oils [5].

2.1.1 Process Description

Visbreaking is a mild process with respect to temperature, and conversion is very low, usually no more than 10%. For thermal cracking, conversion is usually defined as the amount of residue that becomes lighter products after cracking as

shown in equation 2.1.

$$\text{Residue Conversion} = \frac{\text{Feed Residue wt\% - Product Residue wt\%}}{\text{Feed Residue wt\%}} \quad (2.1)$$

If the conditions are too severe, coke formation may become a problem. No catalyst or H_2 is added during the process. The operating variables in visbreaking are temperature and residence time as given below. Two types of visbreaking processes are used commercially: Coil and Soaker [6].

Coil Visbreaking

Figure 2.1 shows a typical coil visbreaking process. The coil visbreaking process is the higher temperature, shorter residence time process. The coil process is also known as furnace cracking. In the 1930s, visbreakers were mostly coil type. As well, when visbreaking became popular in Europe during the 1960s, coil visbreakers were built [7]. The furnace has two separate zones; a heating zone and a cracking zone. The feedstock is heated to the desired temperature in the heating zone and the conversion occurs in the cracking zone. Typical temperatures for furnace cracking usually range from 475°C to 500°C with residence times of 1 to 3 minutes [8]. Coil visbreakers are favoured by ExxonMobil [9].

Soaker Visbreaking

The soaker visbreaking process is the lower temperature, longer residence time process. An example of this process is shown in Figure 2.2. Unlike furnace cracking, a soaking drum is used to provide the additional residence time. This enables a lower cracking temperature to be used. Early soaker drums had problems with coking so coil visbreakers were used instead [7]. In the soaker process, a furnace is also used, but its purpose is to preheat the feedstock before it enters the soaking drum. Typical temperatures for soaker visbreaking are in the range of 400°C to 450°C. Soaker visbreakers are used worldwide by Shell [10].

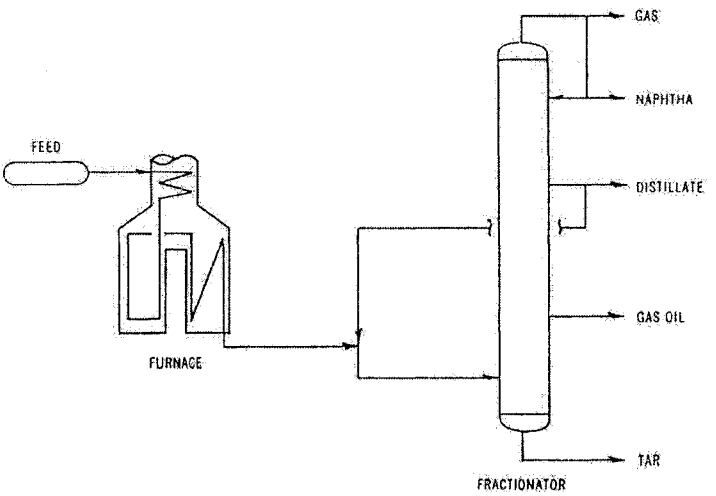

Figure 2.1: Coil Visbreaking Process [9]

After the desired residence times in the furnace or soaking drum, the feed is quenched to terminate cracking, and the product is fractionated into the desired distillate fractions such as naphtha (BP < 170°C), kerosene (BP: 170-250°C), diesel (BP: 250-380°C) and residue (BP > 380°C) as shown in Figure 2.2. Because of the relatively low reaction temperatures and residence times, coking is kept to a minimum during visbreaking. Pressures can range from 50 to 200 psig at the outlet [6]. The conversion of the feed and the properties of the products are generally the same whether the visbreaking was coil or soaker [10].

2.2 Reactive Species in Oil

Previously, many researchers have studied thermal cracking chemistry by pyrolyzing model compounds. The assumption being made with the model compounds is that similar types of compounds and bonds are present in oil and that the behaviour of the model compound under thermal cracking conditions is similar to the compounds and bonds that are present in the oil.

For this work, several model compound pyrolysis studies were chosen from the

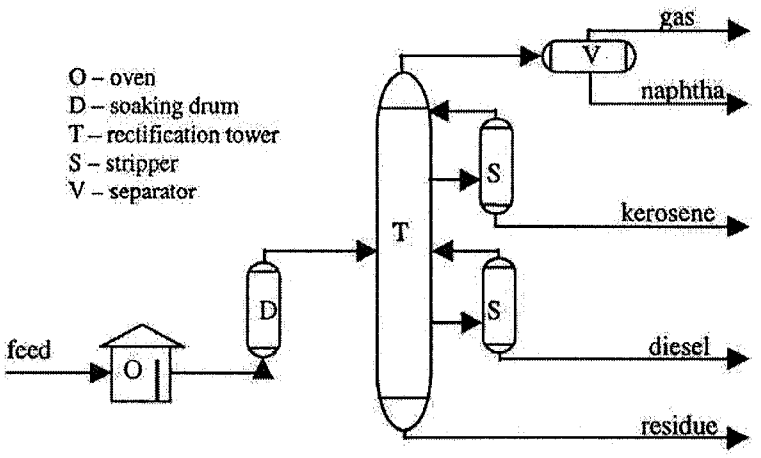

Figure 2.2: Soaker Visbreaking Process [1]

literature to help understand the chemistry of thermal cracking. In total, a hypothetical sulfur compound, 3 aromatic compounds, 2 cycloparaffinic compounds, and 1 hydroaromatic compound were chosen.

2.2.1 α to Sulfides

The α to sulfides bond is shown in Figure 2.3 and the expected bonds to be cracked are marked by the dashed lines. The R-groups (R_1, R_2) shown in Figure 2.3 can be an aromatic, cycloparaffinic, or a chain species.

Figure 2.3: α to Sulfides Bond

Compared to an aliphatic C-C bond (E_A = 84 kcal/mol), an aliphatic C-S (E_A = 77 kcal/mol) has a lower activation energy [11] and contributes to the formation of H_2S. This is not the only form of sulfur that appears in crude oil feedstocks, but it is the only one that is likely to break under visbreaking conditions. Other forms of sulfur include thiophenic (ring) sulfur, but under the mild thermal conditions used

in this study, that form of sulfur is unlikely to crack because it is in a more stable form.

2.2.2 n-Pentadecylbenzene

The first aromatic model compound chosen was n-pentadecylbenzene (PDB). A pyrolysis study of PDB was performed by Savage and Klein (1987) [12]. This compound consists of a benzene ring with a 15-carbon paraffin chain attached and is shown in Figure 2.4.

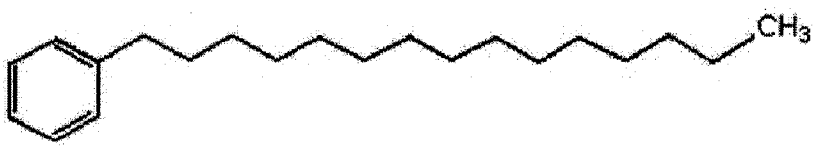

Figure 2.4: n-Pentadecylbenzene Molecule

The long paraffin chain was chosen to allow for maximum product possibilities. The predominant products of the pyrolysis of PDB is toluene and tetradecene. Toluene makes up approximately 30% of the overall products. Styrene, ethylbenzene and tridecane were formed as minor products. The products are summarized in Figure 2.5.

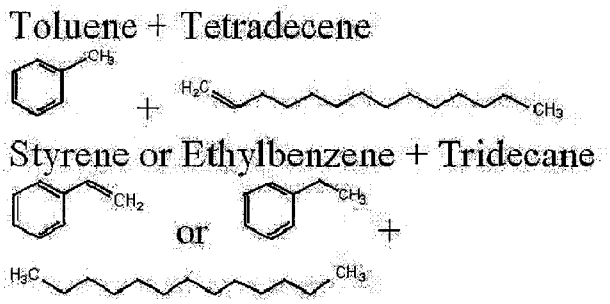

Figure 2.5: Predominant Pyrolysis Products of n-Pentadecylbenzene

2.2.3 1-Undecylnaphthalene

The second aromatic model compound chosen for this study was 1-undecylnaphthalene (UDN). A pyrolysis study of UDN was performed by Smith and Savage (1991) [13]. This compound consists of 2 benzene rings fused together with an 11-carbon paraffin chain attached and is shown in Figure 2.6.

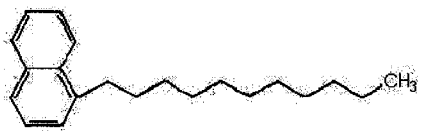

Figure 2.6: 1-Undecylnaphthalene Molecule

The predominant products of the pyrolysis of UDN is methylnaphthalene and decene with methylnaphthalene making up approximately 40% of the overall products. Vinylnaphthalene, ethylnaphthalene and nonane were formed as minor products. The products are summarized in Figure 2.7.

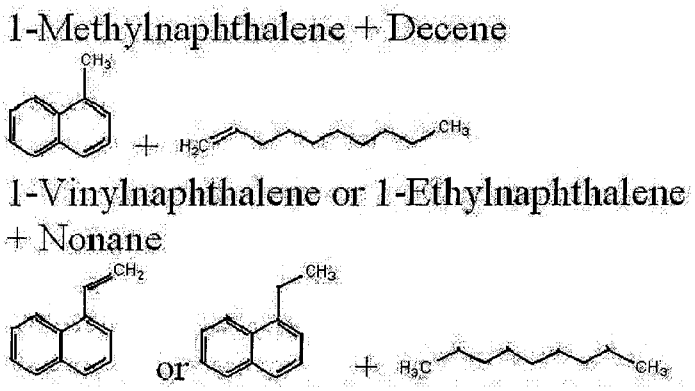

Figure 2.7: Predominant Pyrolysis Products of 1-Undecylnaphthalene

2.2.4 1-Dodecylpyrene

The third aromatic compound chosen was 1-dodecylpyrene (DDP). A pyrolysis study of DDP was performed by Savage et. al. (1989) [14]. This compound consists

of 4 aromatic rings fused together with a 12-carbon paraffin chain attached and is shown in Figure 2.8.

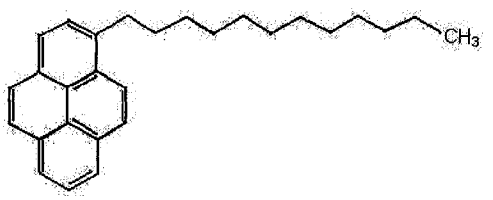

Figure 2.8: 1-Dodecylpyrene Molecule

The predominant products of the pyrolysis of DDP are pyrene and dodecane and methylpyrene and undecene. The products are summarized in Figure 2.9. More methylpyrene is present at lower conversions while more pyrene is present at higher conversions.

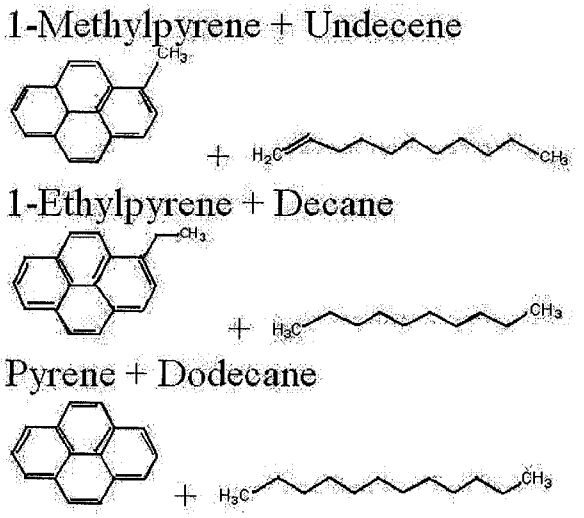

Figure 2.9: Predominant Pyrolysis Products of 1-Dodecylpyrene

2.2.5 n-Tridecylcyclohexane

The first cycloparaffinic compound chosen was n-tridecyclohexane (TDC). A pyrolysis study of TDC was performed by Savage and Klein (1988) [15]. This

compound consists of a cyclohexane ring with a 13-carbon paraffin chain attached and is shown in Figure 2.10.

Figure 2.10: n-Tridecylcyclohexane Molecule

The predominant products of the pyrolysis of TDC are cyclohexane and tridecene and methylenecyclohexane and dodecane. Methylcyclohexane and dodecene were also formed as minor products. The products are summarized in Figure 2.11.

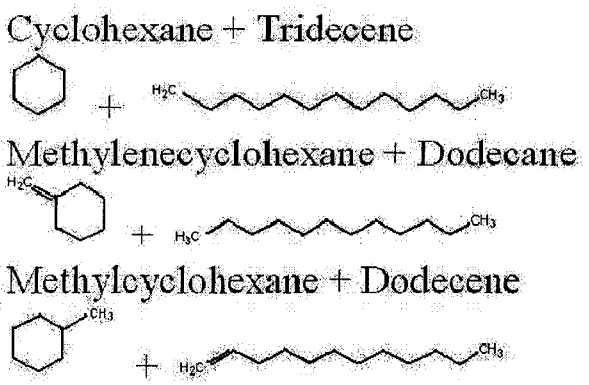

Figure 2.11: Predominant Pyrolysis Products of n-Tridecylcyclohexane

2.2.6 1-Undecyldecalin

The second of the cycloparaffinic compounds chosen was 1-undecyldecalin (UDD), otherwise known as 1-undecylperhydronaphthalene. A pyrolysis study of UDD was performed by Mizan et. al. (1997) [16]. This compound consists of 2 cycloparaffinic rings fused together with an 11-carbon paraffin chain attached and is shown in Figure 2.12.

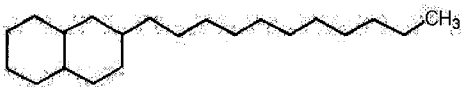

Figure 2.12: 1-Undecyldecalin Molecule

The predominant products of UDD pyrolysis are octahydronaphthalene and undecane, 1-methylenedecalin and decane, and decalin and undecene. The products are summarized in Figure 2.13.

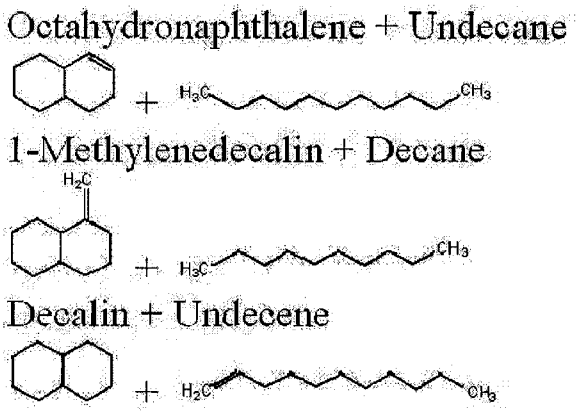

Figure 2.13: Predominant Pyrolysis Products of 1-Undecyldecalin

2.2.7 2-Ethyltetralin

Finally, the hydroaromatic model compound chosen was 2-ethyltetralin (2ET). A pyrolysis study of 2ET was performed by Savage and Klein (1988) [15]. This compound is a hydroaromatic consisting of an aromatic ring fused together with a cycloparaffin ring with an ethyl branch attached and is shown in Figure 2.14.

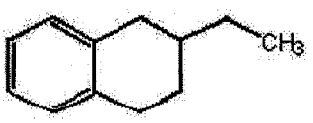

Figure 2.14: 2-Ethyltetralin Molecule

The main products of the pyrolysis of 2ET are naphthalene and C_2 gas, 2-ethylnaphthalene, dialin and C_2 gas, and 2-ethyldialin. At lower temperatures, more 2-ethylnaphthalene was present while at higher temperatures, naphthalene was the dominant product [15]. The products are summarized in Figure 2.15.

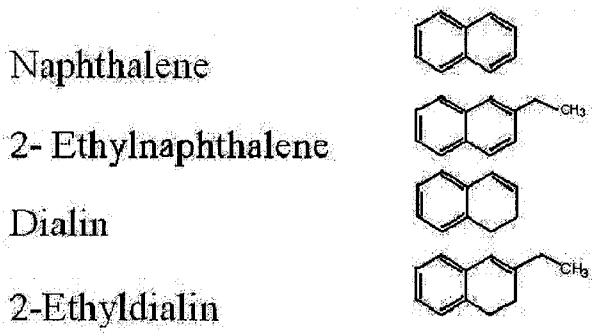

Figure 2.15: Predominant Pyrolysis Products of 2-Ethyltetralin

This compound was chosen to represent the dehydrogenation of cycloparaffin rings into aromatic rings. A cycloparaffin ring is more likely to dehydrogenate when in close proximity to an aromatic ring than by itself under mild thermal conditions. In fact, from pyrolysis of n-tridecylcyclohexane, toluene was not formed below 450°C [15], which is above the temperatures used in this study.

2.2.8 Relative Reactivity

The Arrhenius parameters for the pyrolysis of the model compounds are shown in Table 2.1. Arrhenius data for the sulfur compound was not available.

Interestingly, from comparing the reaction rate constants in Table 2.1, the heaviest compound, DDP, was the most reactive compound while the least reactive compound was 2ET. If it is assumed that the relative reactivities of the model compounds are similar for the oil, then it would be expected that the larger polyaromatic ring compounds will be the most reactive.

Table 2.1: Model Compound Arrhenius Parameters

Compound	A_o (s^{-1})	E_A (kcal/mol)	k(400°C) (s^{-1})
DDP	3.89 x 10^{16}	62.25	2.39 x 10^{-4}
PDB	1.10 x 10^{14}	55.45	1.09 x 10^{-4}
UDD	7.90 x 10^{10}	46.5	6.30 x 10^{-5}
UDN	3.49 x 10^{14}	58.14	4.63 x 10^{-5}
TDC	7.90 x 10^{14}	59.4	4.08 x 10^{-5}
2ET	5.00 x 10^{12}	53.5	2.13 x 10^{-5}

2.3 Carbon Bond Reactivity in Oil

To be able to monitor the thermal cracking chemistry occurring during visbreaking, there is a need to quantify the reactive bonds identified from model compounds. Pyrolysis of the model compounds gives information about which ones are the reactive bonds. These bonds are the α to sulfides, $\alpha\beta$ to aromatic, and α to cycloparaffin bonds. Cycloparaffin dehydrogenation can also be monitored. As previously mentioned, the breaking of the α to sulfide bonds contributes to the formation of H_2S, monitored as a gas product. The changes in content of these bonds and others given below from the feed to product indicate that cracking has occurred. The assumption being made here is that the bond types in the oil will have similar relative reactivities to those of the model compounds.

2.3.1 $\alpha\beta$ to Aromatic

The second bond type is the $\alpha\beta$ to aromatic bond. An example of this bond is marked by the dashed line on Figure 2.16.

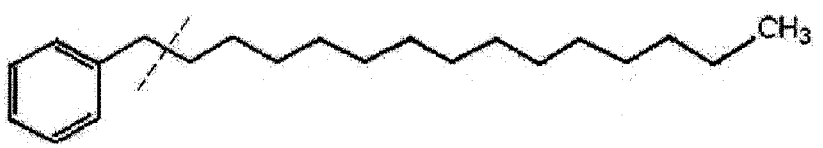

Figure 2.16: $\alpha\beta$ to Aromatic Bond

As shown previously in Figure 2.4, the major aromatic products of the pyrolysis of PDB are toluene, styrene and ethylbenzene. When these products are formed, there is a decrease in the amount of the $\alpha\beta$-aromatic bond. If ethylbenzene is formed, the ethyl carbon on the chain is classified as an ethyl-aromatic and not an $\alpha\beta$-aromatic carbon. Similarly, for the pyrolysis of UDN and DDP, the major products formed also result in a decrease in the amount of the $\alpha\beta$-aromatic bond. Significant cracking also occurs at the α-aromatic bond for DDP. Thus, for 1-ring and 2-ring aromatic compounds, the most likely bond to break under thermal cracking conditions is the $\alpha\beta$-aromatic bond. For the 4-ring aromatic compound, cracking is also likely to occur at the α-aromatic bond as well as at the $\alpha\beta$-aromatic bond. Cleavage of this bond could result in long chains from the residue fraction ending up in the gas oil fraction as discussed below.

2.3.2 α to Cycloparaffin

The third bond type is the α to cycloparaffin bond. An example of this bond is marked by the dashed line on Figure 2.17.

Figure 2.17: α to Cycloparaffin Bond

As previously mentioned, the primary cycloparaffinic products from TDC pyrolysis are cyclohexane and methylenecyclohexane. Both of these products cause a loss of the α-cycloparaffin bond. For the pyrolysis of UDN, the major products also cause a loss of the α-cycloparaffin bond. Thus, for one-ring and two-ring cycloparaffinic compounds, the bond most likely to break under thermal cracking conditions is the α-cycloparaffinic bond. Multi-ring cycloparaffinic compounds with more than 2 rings were not used for this study because average cycloparaffinic clus-

ter sizes in the feedstock and products had a maximum of 2 rings. As previously seen, when comparing activation energies, the 1-ring cycloparaffinic compound is the second most reactive compound after DDP.

2.3.3 Chain Midsection Carbon

One carbon bond type that has not been mentioned is chain midsection carbon. An example of this bond type is shown in Figure 2.18. The chain midsection carbons are marked by the dots (•). This type of carbon is paraffinic carbon in between two ends. An end can be an aromatic, cycloparaffinic, branched-paraffinic, sulfur, olefin or terminal methyl carbon.

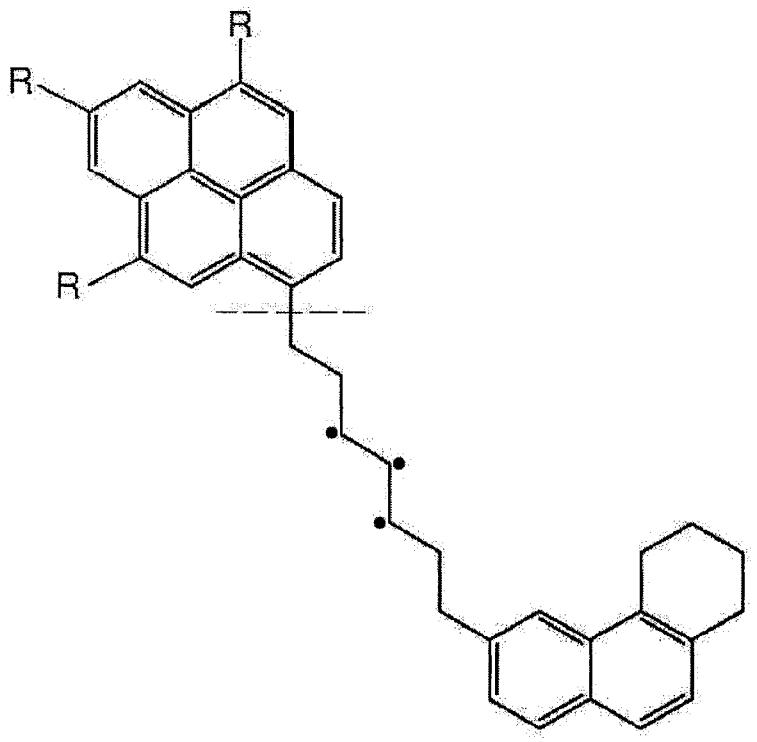

Figure 2.18: Chain Midsection Carbon

If cracking occurs on a molecule at the bond marked in Figure 2.18 (α to aromatic) or at the next bond position ($\alpha\beta$ to aromatic), then there is likely to be a

decrease in the amount of chain midsection carbon in the residue and an increase in chain midsection carbon in the gas oil from feed to product. If cracking were to occur in the residue fraction on a bond similar to the one marked by the dashed line in Figure 2.18, the chain midsection carbons may migrate from the residue fraction to the gas oil fraction due to decrease in molecule size. Thus, a decrease in chain midsection carbons in the residue from feed to product and a gain in chain midsection carbons in the gas oil is likely to indicate thermal cracking.

2.3.4 Cycloparaffin Dehydrogenation

Finally, there is cycloparaffin dehydrogenation. Opening of cycloparaffin rings was not considered as there is little cracking of cycloparaffin rings below 480°C [8]. The aromatization of carbon chains was also not considered due to lack of proper conditions [17]. Thus, the only likely source of aromatic increase and cycloparaffin loss would be through dehydrogenation of cycloparaffin rings into aromatic rings. An increase in the amount of aromatic carbon increases density and makes the oil more dense.

2.4 Nuclear Magnetic Resonance Spectroscopy

To be able to quantify the reactive bonds during thermal cracking, nuclear magnetic resonance (NMR) spectroscopy used to characterize to the feedstock and products. NMR spectroscopy is an analytical tool that has been used for analysis of a wide range of compounds. It is one of the few techniques that can be used to study compounds from all three states of matter [18]. When a sample is analyzed using NMR spectroscopy, a spectrum containing peaks at different frequencies is obtained. These peaks indicate what bond types are present in the sample and their relative amounts can be determined based on the areas under those peaks.

2.4.1 Previous Application to Crude Oil and Bitumen

Using NMR spectroscopy, a structural analysis of a crude oil can be performed. This type of analysis has proven useful for characterizing and studying crude oils. Previously, the data obtained from NMR spectroscopy has been used in 3 different ways [19].

Average Structural Parameters

The first approach that has been previously employed is calculation of average structual parameters. In this approach, parameters such as aromaticity, average alkyl chain length, average number of aromatic and cycloparaffin rings per molecule, and fraction of saturate carbon are estimated. In total, approximately 12-15 parameters are usually estimated. For this approach, four different methods have been proposed to estimate average structural parameters. The first method was proposed by Williams (1958) using data from ^{1}H NMR spectra to calculate average parameters [20]. The second method is the method of Brown and Ladner (1960) [21] who used data from ^{1}H NMR spectra as well as elemental analysis to estimate aromaticity and degree of aromatic substitution. The method proposed by Knight (1967) uses data from ^{13}C NMR spectra to estimate aromaticity and many other parameters [22]. Finally, the method proposed by Clutter et. al. (1972) uses data from ^{1}H NMR spectra to calculate the same parameters from the method proposed by Williams (1958) as well as the fraction of fused ring systems, average molecular weight and average molecular formula [23]. The methods of Williams, Knight, and Clutter et. al. were applied only to aromatic fractions of oil.

There are many examples of researchers using ^{1}H and ^{13}C NMR spectroscopy to calculate average structural parameters of various oils and fractions [24], [25], [26], [27].

Representative Molecular Structures

The second approach is average molecule estimation. The goal of this approach is to generate molecular structures that are representative of the carbon and hydrogen distributions of the oil. For example, if 45% of carbon in an oil was aromatic and 30% of its hydrogen was aromatic, an estimated molecular structure would have similar values. In this approach, both ^{1}H and ^{13}C NMR spectroscopy are applied to determine the amount of aromatic and aliphatic carbon, α-hydrogen, β-hydrogen, γ-hydrogen and aromatic hydrogen as well as the nitrogen and sulfur in an average molecule [19]. Once this information is known, an average molecular formula is estimated. From there, molecular structures can be generated.

Generation of structures is usually done with computers. Structures can be generated via an algorithm. Either way, generated structures that do not match the data from NMR spectra are discarded. This approach usually generates a handful of structures that match the data from NMR spectra. These average structures can be used to estimate thermodynamic and physical properties of the oil using group contribution methods [28]. The assumption is that the properties of the molecular structures will be similar to that of the original oil or fraction.

This approach has been employed recently to attempt to estimate molecular structures of Athabasca asphaltenes [29], and fractions of Kuwaiti crude oil [30], [31]. Also, Michael et. al. (2005) [32] applied NMR spectroscopy to investigate the differences in average chemical structures of asphaltenes before and after thermal processing.

Functional Group Analysis

The final approach is called Functional Group Analysis. The idea of this approach is to choose functional groups that may represent structures that exist in oil. With the chosen functional groups, the concentrations of the functional groups

are estimated to try and match the structural characteristics of the oil. From this information, it is hoped that a structural profile of the oil can be generated [19].

The functional groups can be species such as a benzene ring, a biphenyl bridge, a diphenylmethane CH_2, or a hydroaromatic like tetralin. Balance equations are written for all the desired structural parameters. From the chosen functional groups, the concentrations of the groups are estimated to match structural characteristics of the oil such as α-hydrogen or aromatic carbon estimated from ^1H and ^{13}C NMR spectroscopy.

This approach has been used to analyze synthetic fuels [33] and compare structural profiles of heavier fractions of various types of feedstocks [34].

2.4.2 Application of NMR Spectroscopy For This Project

In this work, a different approach than the three approaches discussed above was used. It is somewhat similar to functional group analysis, but instead of choosing functional groups, data from both ^1H and ^{13}C NMR as well as elemental analysis were used to quantify individual carbon types in the feed and products. This carbon type analysis was performed on all the liquid pseudo-components in the feed and products. Figure 2.19 shows the aromatic and olefinic carbon types quantified using this technique. Figure 2.20 shows the cycloparaffinic and paraffinic carbon types while Figure 2.21 shows the branch-paraffinic carbon types quantified using NMR spectroscopy. A complete list of the carbon types quantified from NMR spectroscopy can be found in Appendix A.

Looking at Figure 2.19, there are several different aromatic and olefinic carbon types. Carbon type 1 refers to aromatic bridge carbon. These are the carbons that join multiple aromatic rings together. Carbon type 2 is aromatic alkyl substituted carbon. These are aromatic carbons that have a paraffin or cycloparaffin species attached to them. Carbon type 3 is aromatic CH. These are carbons in an aromatic

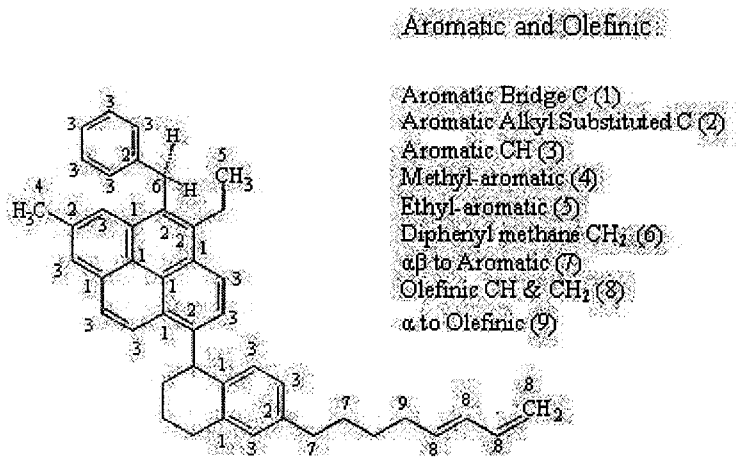

Figure 2.19: Aromatic and Olefinic Carbon Quanitified by NMR Spectroscopy

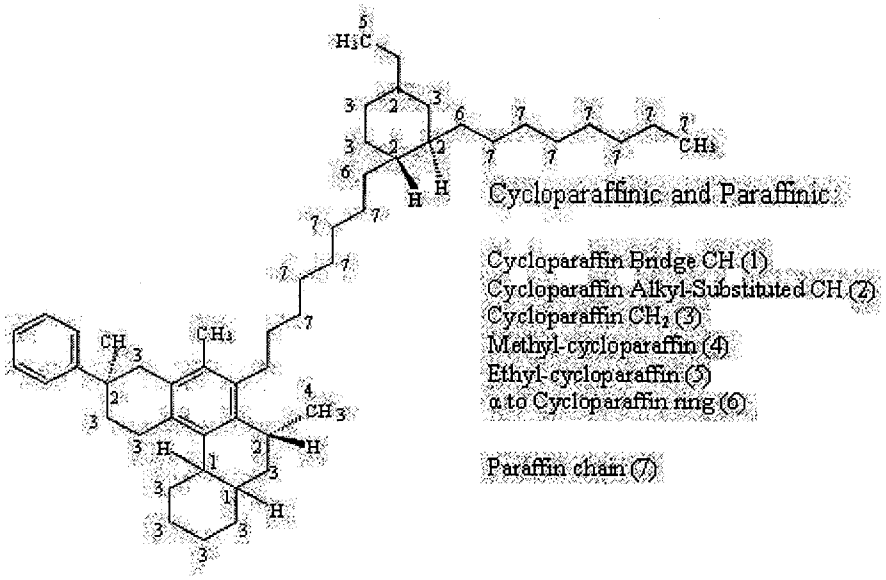

Figure 2.20: Cycloparaffinic and Paraffinic Carbon Quantified by NMR Spectroscopy

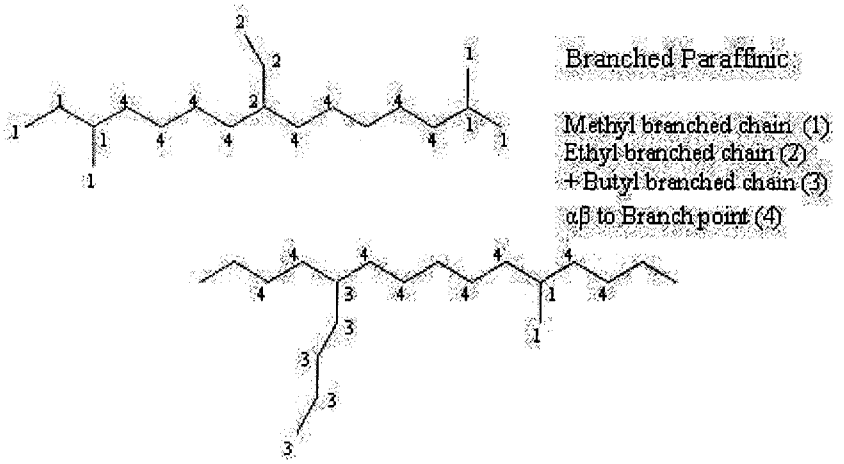

Figure 2.21: Branch-Paraffinic Carbon Quantified by NMR Spectroscopy

ring that are not substituted. Carbon types 4 and 5 are methyl-aromatic and ethyl-aromatic carbon, respectively. They are methyl and ethyl groups attached to an aromatic carbon. Carbon type 6 is the carbon in diphenylmethane CH_2. When two aromatic rings are separated by a methylene bridge, the carbon type in the bridge is a diphenylmethane CH_2. Carbon type 7 is α and β to aromatic carbon. These are the first two carbons of a chain that is at least 4 carbons long attached to an aromatic ring. The α and β refer to the first and second bond positions from the ring, respectively. Carbon type 8 is olefinic carbon and includes both olefinic CH and CH_2. Carbon type 9 is α to olefinic carbon. This refers to a paraffinic carbon that is adjacent to an olefinic carbon. The carbon types in Figure 2.20 follows the same logic except that cycloparaffin ring carbon is CH_2 instead of CH. Also, the cycloparaffin bridge and alkyl substituted cycloparaffin ring carbons are CH instead of C. The carbon types in Figure 2.21 are methyl, ethyl, +butyl branched chains, and α and β to branch points that are aliphatic CH species.

The molecules shown in Figures 2.19, 2.20, and 2.21 are not actual molecules found in the crude oil feedstocks, but are only intended to be illustrative to show the carbon types that can be identified and quantified using NMR spectroscopy. This

information provides a new level of detail and shows that NMR spectroscopy can be a powerful tool for characterizing crude oil feedstocks.

2.5 Previous Visbreaking Models

The modeling and simulation of thermal cracking processes is a complex task due to the lack of well-defined components within the feedstock. Because of this, the most common approach to modeling is defining pseudo-components based on physical properties such as boiling point or molecular weight. The kinetics of the process are then estimated based on those pseudo-components.

Different forms of visbreaking models have been previously proposed. The first type consists of a single reaction that converts the feed to a product.

$$\text{Feed} \longrightarrow \text{Product}$$

Examples of this form of model have been previously presented. Here, the pseudo-components are the feed and product. A model proposed by Shu and Venkatesan [35] used Cold Lake Bitumen as its feedstock. The Arrhenius parameters were estimated to be $A_o = 8.18 \times 10^9$ hr^{-1} and $E_A = 31.2$ kcal/mol. The yield of the product gas oil (BP: 204-538°C) and residue (BP > 538°C) fractions were correlated with heating time and found to be linear for the range of heating times used. In addition, a viscosity function was also correlated to the rate constant, k. This allowed the kinetic constant for visbreaking to be estimated given viscosity measurements of the feed and products. The viscosity function method was also tested on Athabasca bitumen and the model seemed to represent the data well.

A model proposed by Krishna et. al. [36] used Agjahari Long Residue as its feedstock. Visbreaking experiments were carried out at temperatures ranging from 427-450°C. The Arrhenius parameters estimated were $A_o = 2.17 \times 10^{12}$ s^{-1} and $E_A = 53.7$ kcal/mol. The yields of various distillate fractions were also measured

as a function of conversion. The gas yield and yield of the IBP to 150°C fraction were linear while the yields of the 250-370°C and 370-500°C fractions were not for the range of conversions obtained. Also, the effect of conversion on the Conradson carbon residue of the 370°C+ fraction and the viscosity at 50°C of the product were investigated.

Another model proposed by Al-Soufi et. al. [37] involved visbreaking of a heavy Iraqi residue. Visbreaking was studied at four different temperatures ranging from 435 to 480°C and residence times ranging from 43 to 109 seconds in the coil and 151 to 397 seconds in the soaker visbreakers. The estimated activation energy for the feedstock was E_A = 23.7 kcal/mol. No pre-exponential factor (A_o) was estimated. Yields of distillate fractions were measured versus conversion and were found to be linear for the range of conversions obtained. The effect of reaction time and temperature on the percentage decrease in viscosity, flash point, and pour point were also investigated.

In all three cases, the apparent kinetics of visbreaking seemed to be first order. Arrhenius parameters were estimated for all three feedstocks and the results were all quite different. The yields of the product distillate fractions were measured but not estimated directly from the reaction network.

More recently, models of the following form have been proposed.

Feed $\longrightarrow$ Various Distillate Fractions

As well, reactions between the product distillate fractions were sometimes included.

For Singh et. al. [38], 4 different Indian feedstocks were used. Two were vacuum residues, one was a vacuum residue blended with oil fluxes and the last was asphalt from a deasphalting process. The product distillate fractions were gas (G), gasoline (GLN) (BP < 150°C), light gas oil (LGO) (BP: 150-350°C), and vacuum gas oil (VGO) (BP: 350-500°C). The residence times ranged from 3 to 15 minutes and the temperatures ranged from 400 to 430°C. The final reaction network consists

of 6 reactions with a 7th reaction that becomes significant at 430°C as shown in Figure 2.22. For the six main reactions, Arrhenius parameters were estimated for each of the four feedstocks. An error analysis showed that 76-85% of the predicted values were within 30% error.

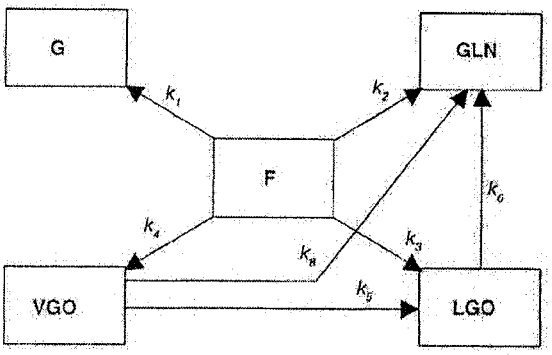

Figure 2.22: Reaction Network for Singh et. al. [38]

For Kataria et. al. [39], the feedstocks used were three vacuum residues, two asphalts, and a vacuum bottoms Feed so the distillate products were gas, gasoline, light gas oil, and vacuum gas oil. The boiling point ranges for the distillate fractions were the same as the ones given above from Singh et. al. [38]. Batch residence time ranged from 0-15 minutes and temperatures ranged from 400-430°C. The reaction network was very similar to that of Singh et. al. [38] with 7 reactions and is shown in Figure 2.23. Arrhenius parameters for each reaction in the reaction network were estimated for each feedstock by using minimization functions. The yields of the distillate fractions were also correlated with severity index, a concept that will be introduced later in this chapter.

Both of the models presented above give information about conversion of the feed into the individual distillate fractions in the product. Along with the single reaction models, the product yields are estimated from a reaction network with estimated kinetic parameters for each reaction within the network. For the single reaction models, kinetic parameters were estimated for each feedstock and were all

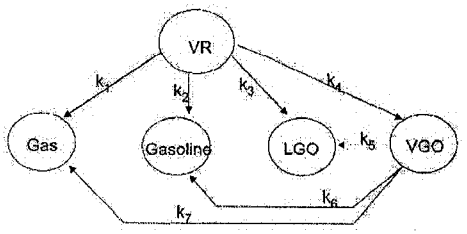

Figure 2.23: Reaction Network for Kataria et. al. [39]

different. This shows that any kinetic parameters estimated for a given feedstock are not applicable to other feedstocks.

Although reaction network models do give information about the yield of product distillate fractions, they do not give any information on the types of chemical reactions that occur within the fractions themselves. In other words, no information about the thermal chemistry of the feedstocks or products is included or utilized. Thermal chemistry knowledge is vital to understanding thermal cracking processes and attempts should be made to include this information in thermal cracking models.

2.5.1 New Pseudo-Component Definition

Pseudo-components are necessary when modeling the thermal cracking of oil because oil's complex nature does not permit an exact composition to be known. Pseudo-components are normally based totally on physical properties without chemistry information. A common method for defining pseudo-components is to obtain a boiling curve and dividing it into boiling point cuts or ranges. This was the method for defining pseudo-components in the thermal cracking models discussed previously. In the current work, pseudo-components that include chemistry information are defined.

First, the feed and products were fractionated by distillation into a gas phase, naphtha (BP $< 204^{o}$C), gas oil (BP: 204-524^{o}C), and residue (BP $> 524^{o}$C). Then,

the gas oil and residue fractions were fractionated further by polarity using the SARA (Saturates, Aromatics, Resins, Asphaltenes) protocol. For this study, the resins were referred to as polars and combined with the aromatics. Asphaltenes, the fraction of a feedstock not soluble in a paraffin solvent such as pentane or heptane, are the heaviest component of the oil so they only appear in the residue fraction.

The gas phase and naphtha fraction were not fractionated by polarity like the gas oil and residue were. Table 2.2 gives a summary of the pseudo-component definitions. In total, 7 pseudo-components were defined. The abbreviations for each pseudo-component listed in Table 2.2 will be used instead of the names in the rest of this thesis.

Table 2.2: Summary of Pseudo-Components

Gas
Naphtha (N)
Gas Oil Saturates (GO-S)
Gas Oil Aromatics+Polars (GO-A+P)
Residue Saturates (R-S)
Residue Aromatics+Polars (R-A+P)
Residue Asphaltenes (R-As)

These pseudo-component definitions are less arbitrary than just choosing boiling point ranges as pseudo-components. They provide some insight into the chemistry of each pseudo-component. By defining pseudo-components in this way, similar carbon types were grouped together. For example, the GO-S pseudo-component would contain cycloparaffinic and paraffinic carbons and very few, if any, aromatic carbons. The GO-A+P pseudo-component would mostly contain aromatic rings with paraffinic chains attached. The R-A+P and R-As pseudo-components would contain similar carbon types as the GO-A+P pseudo-component, but with larger aromatic ring clusters. The GO-A+P, R-A+P, and R-As would likely also contain aromatic rings attached to cycloparaffinic rings as well. Carbon type analyses from

NMR spectroscopy allow the quantification of each of those carbon types in each of the pseudo-components. This information is useful for understanding visbreaking thermal chemistry.

2.6 Process Severity

Severity is a concept that is meant to be a measure of process conditions, particularly including process temperature, pressure, and residence time. Being able to predict conversions and product yields is the purpose of this concept. Previously, many different severity factor or parameter equations have been proposed. Some of the early measures proposed included coil outlet temperature, yield ratios (e.g. methane yield/propylene yield), feed gasification (e.g. C_3 and lighter yield), and decomposition of model compounds [40]. A review of more complex severity factors and parameters was done by Van Camp et. al. (1985) [41].

2.6.1 Visbreaking Severity

The simplest description of process severity was proposed by Yan (1990) [42] and was based on the observation that visbreaking has apparent first order kinetics. For a first order reaction in a plug flow reactor, conversion is calculated as

$$ln(1 - X) = -k\tau \tag{2.2}$$

$$k = A_o exp\left(\frac{-E_A}{RT}\right) \tag{2.3}$$

where X is conversion, k is the first order reaction rate (s^{-1}), τ is the reactor residence time in seconds, A_o is the Arrhenius pre-exponential factor (s^{-1}), E_A is the activation energy in J/mol, R is the universal gas constant in $J/mol \bullet K$, and T is the temperature in Kelvin. The activation energy for Athabasca bitumen was defined to be 242.7 kJ/mol.

Theoretically, a desired conversion can be achieved with different combinations of temperature and residence time. Assuming the reaction rates follow an Arrhenius relationship, the temperature will have an effect on reaction rates. Yan (1990) [42] proposed that the severity of visbreaking can be expressed as equivalent residence time (ERT) and defined as:

$$ERT = \left(\frac{k_T}{k_{427}}\right)\tau \tag{2.4}$$

where k_T is the reaction rate constant at a given temperature and k_{427} is the reaction rate constant at 427°C (700 K). In this expression, 700 K is defined as the reference temperature.

Substituting the Arrhenius expressions for the reaction rates into equation 2.4 gives

$$\frac{k_T}{k_{427}} = exp\left(-\frac{E_A}{R}\left(\frac{1}{T} - \frac{1}{700}\right)\right) \tag{2.5}$$

Equation 2.5 was derived by dividing the Arrhenius expression for a given temperature by the Arrhenius expression at 700 K. Since the pre-exponential factor (A_o) is constant, it does not appear in the severity index expression.

Finally, substituting equation 2.5 into equation 2.4 and rearranging gives the following expression for ERT:

$$ERT = \tau\ exp\left(-\frac{E_A}{R}\left(\frac{1}{T} - \frac{1}{700}\right)\right) = \tau\ exp\left(-\frac{E_A}{R}\left(\frac{700 - T}{700T}\right)\right) \tag{2.6}$$

From here, ERT will be referred to as severity index (SI). The severity at other temperatures is expressed as an equivalent residence time at 427°C. Thus, different combinations of temperatures and residence time are standardized to an equivalent residence time at 427°C. This enables a direct comparison of severity at different temperatures and residence times.

2.6.2 Application of Severity Index for Product Yield Correlation

This definition of severity index was correlated with the yields of distillate fractions for low severity visbreaking of various Indian residues and asphalts by Kataria et. al. [39]. Yields for all five distillate fractions shown in Figure 2.23 were correlated with severity index and other properties such as Conradson carbon residue content, pentane and heptane insolubles content, and saturates content. The correlation coefficient (R^2) values for the yield correlations ranged from 0.71 to 0.88, suggesting the predicted yields of the distillate fractions had acceptable agreement with the experimental data.

2.6.3 Model Compounds and Severity Index

The literature data for the model compounds described in Section 2.2 were used to prepare plots of conversion against severity index for the compounds. The conversion profile of all of the model compounds is shown in Figure 2.24. The quantity plotted on the x-axis is SI/1000 and is called reduced severity.

As previously mentioned and shown in Figure 2.24, DDP is the most reactive compound. The conversion of DDP seems to be asymptotically approaching 1 at the severities used in this study while the conversion of the other model compounds is still increasing linearly in the range of severities used in this study.

2.7 Proposed Method

Overall, for model development, several model compounds were chosen from the literature and represent the types of species that are found in oil. The pyrolysis of the model compounds gives information about reactive bond behaviour under thermal cracking conditions. Reactive carbon-carbon bond cleavage was quantified from feed to product using NMR carbon type analysis. A new method of defining

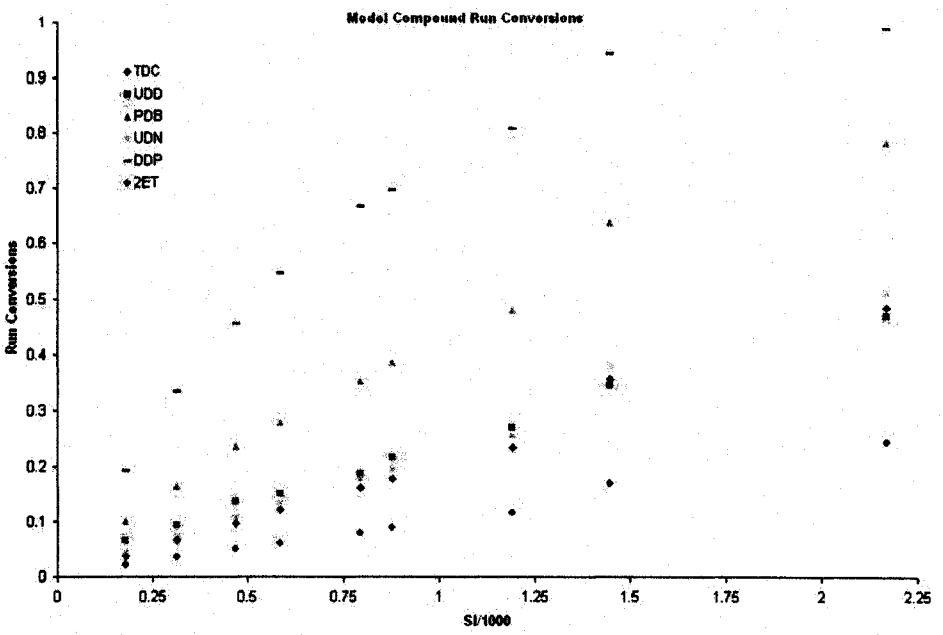

Figure 2.24: Model Compound Run Conversions

pseudo-components that included and utilized chemistry information was also introduced. With this data, major thermal cracking reaction pathways were identified. The yields of the distillate fractions, major carbon types, and coke formation were correlated with severity index. Thus, the current work presents a model consisting of two parts: reaction pathways that describe the formation of light end products and the use of severity index to predict yields and compositions of the products generated during the visbreaking of Athabasca bitumen.

Chapter 3

Experimental Methods

This chapter describes the steps used for fraction preparation and characterization as well as the experimental conditions. The actual visbreaking experiments, fraction preparation and characterization, acquisition of NMR spectra, and spectra analyses were performed by the staff at the National Centre for Upgrading Technology (NCUT) in Devon, Alberta, Canada.

3.1 Fraction Preparation

The feedstock used for this study was Athabasca bitumen from the Underground Test Facility (UTF). Athabasca bitumen is an extra-heavy feed with a high sulfur content (~5%). The feed and total liquid products (TLP) were fractionated into naphtha (BP < 204°C), gas oil (BP: 204-524°C), and residue (BP > 524°C) using the American Society for Testing and Materials (ASTM) D1160 method [43].

Asphaltenes were precipitated from the D1160 vacuum residues (BP > 524°C) with pentane, using a single treatment of the procedure outlined in Peramanu et. al. (1999) [44]. This method included adding 40 volumes of pentane, sonicating in a bath sonicator for 45 minutes, leaving the mixture to rest overnight at room temperature, then sonicating for an additional 30 minutes before filtering and washing with pentane until the eluent is colourless. The solids (asphaltenes) were dried in a

vacuum oven at 45°C until constant weight was obtained. The pentane solvent was removed from the eluent (maltenes) by rotoevaporation followed by drying in the vacuum oven at 45°C.

The gas oil and the residue maltenes were separated into saturates and aromatics+polars fractions using a modification of the clay-gel adsorption chromatography method described in Peramanu et. al. (1999) [44]. After collection of the saturates sample using pentane, the polar fraction was adsorbed to the upper attapulgus clay while the aromatics fraction adsorbed to the lower silica gel column. The columns were separated and the aromatics eluted from the silica gel by washing with 2.5 volumes of methylene chloride. The polars were removed from the clay by washing successively with 3.3 volumes of methylene chloride, 3.3 volumes of methanol:methylene chloride (60:40) and finally with 1.7 volumes of methanol. The aromatic and polar fractions were pooled, rotoevaporated to constant volume, then dried in a 45°C vacuum oven until constant weight was obtained.

3.2 Fraction Characterization

3.2.1 Gas and Naphtha Component Analysis

Refinery gas analysis was run on the gas product on either a Refinery Gas Analyzer (MTI) or Agilent Technologies 3000A gas chromatography (GC) instrument. PIONA (paraffin, isoparaffin, olefin, naphthene, and aromatic) analyses of the naphtha products were performed on an Agilent Technologies 6890 GC instrument.

3.2.2 Elemental Analyses

Sulfur contents of naphtha were measured using x-ray fluorescence (ASTM D4294) on a Horiba XR Fluorometer (SLFA-1800). The sulfur contents of the gas oil saturates were measured by GC (Agilent Technologies 6890) using sulfur chemiluminescence detection (ASTM D5623). The sulfur contents of all other

samples were measured using a Leco SC 432 analyzer where ASTM D1552 was used for the aromatics+polars and ASTM D4239 was used for asphaltenes. The nitrogen contents of the naphtha and saturates were measured using the ASTM D4629 method on a Dohrman Nitrogen Analyzer (DN-1000). The carbon and hydrogen contents of the saturates were measured using the ASTM D5291 method on a Perkin Elmer 2400 analyzer. The carbon, hydrogen, and nitrogen contents of the aromatics+polars and asphaltenes were measured on a Leco 1000 Analyzer using ASTM D5291 for the aromatics+polars and ASTM D5373 for the asphaltenes. The carbon and hydrogen contents of the naphtha were measured on the Leco 1000 Analyzer using the ASTM D5291 procedure.

3.2.3 Nuclear Magnetic Resonance Spectroscopy

NMR analyses were performed at room temperature (19 $\pm$ 1°C) on a Varian Unity Inova 600 NMR spectrometer, operating at 599.733 MHz for proton (^{1}H) and 150.817 MHz for carbon (^{13}C). For proton, 20 mg quantities were dissolved in 700 μL deutero-chloroform. For carbon, 50 mg quantities of asphaltenes were dissolved in 700 μL deutero-chloroform while 100 mg or μL quantities of the other samples were dissolved in 600 μL deutero-chloroform. Both proton and carbon spectra were run using a Varian 5 mm broadband ^{13}C{^{1}H} probe.

The quantitative carbon spectra were acquired using an acquisition time of 1.0 s and a sweep width of 36003.6 Hz. For residue samples, a flip angle of 35° (4.6 μs) and a relaxation time of 5 s were used. For naphtha and gas oil samples, a flip angle of 26.4° (3.4 μs) and a relaxation time of 10 s were used. Reverse-gated waltz proton decoupling was used to avoid nuclear Overhauser effect enhancements of the protonated carbon signals. The spectra were the result of 2048 scans. Line broadening of 5 Hz for the naphtha, 10 Hz for the gas oil, and 15 Hz for the residue samples was used to improve the signal-to-noise ratio of the spectra. The spectra

were referenced to the deutero-chloroform resonance being set to 77 ppm.

The quantitative proton spectra were acquired using an acquisition time of 3 s and a sweep width of 20000 Hz. A flip angle of 30.6° and no relaxation time were used. The spectra were the result of 128 scans. Line broadening of 0.33 Hz was used to improve the signal-to-noise ration of the spectra. The spectra were referenced to the deutero-chloroform resonance being set to 7.24 ppm. Spectra were processed using a procedure based on that described by Japanwala et. al. [45].

3.3 Visbreaker Operating Conditions

The experimental visbreaker was operated as a soaker visbreaker. A total of 9 Athabasca bitumen visbreaking runs were performed at 5 different temperatures, 2 feed flow rates, and 2 residence times. The reactor pressure was set at 1 MPa. A summary of the operating conditions for each run is listed in Table 3.1.

Table 3.1: Visbreaker Experimental Conditions

Run	Temperature (°C)	Flow Rate (kg/h)	Residence Time (min)
1	390	2	30
2	405	2	30
3	405	3	20
4	420	3	20
5	420	2	30
6	415	2	30
7	415	3	20
8	430	3	20
9	430	2	30

The results of the analyses of Run 1 were not within 2 standard deviations so the data from Run 1 was removed from consideration for model development.

3.3.1 Visbreaking Reactor Dimensions

The reactor's length was 95 inches with a diameter of 0.965 inches. The run temperatures listed in Table 3.1 were average temperatures over the length of the reactor. The reactor was heated to maintain the required temperature for each run.

Chapter 4

Feed and Product Characterization

4.1 Feed and Product Characterization

This chapter presents results from the characterization of the feed and product. The feed and product characterization was performed by the staff at the National Centre for Upgrading Technology (NCUT) in Devon, Alberta, Canada.

4.1.1 Severity Index

The severity index for each run was calculated from equation 2.6 and the results are shown in Table 4.1. The data presented are also listed in order of severity from lowest to highest. This is also done throughout the thesis to show the trends in the data with increasing severity.

As seen in Table 4.1, the experimental runs were not performed in order of increasing severity. This was done to reduce experimental bias by randomizing uncontrolled factors that may have an impact on experimental results.

4.1.2 Elemental Analysis

Table 4.2 shows the results of the elemental analyses performed on the feed and product runs. The hydrogen to carbon (H/C) ratios are also shown in Table 4.2.

Table 4.1: Severity Index

Run	Severity Index (sec)
3	313.1
2	469.6
7	585.2
4	794.7
6	877.8
5	1192.1
8	1446.5
9	2169.7

Table 4.2: Feed and Product Elemental Analysis

	Mass Fractions				
Run	Carbon	Hydrogen	Nitrogen	Sulfur	H/C Ratio
Feed	0.843	0.103	0.0039	0.046	1.45
3	0.843	0.100	0.0044	0.052	1.42
2	0.832	0.107	0.0038	0.055	1.46
7	0.842	0.100	0.0041	0.052	1.42
4	0.839	0.103	0.0038	0.052	1.46
6	0.837	0.103	0.0041	0.053	1.47
5	0.838	0.101	0.0043	0.054	1.44
8	0.837	0.104	0.0039	0.053	1.48
9	0.831	0.107	0.0042	0.057	1.53

Oxygen content in the feed and product was not measured and thus was not part of the elemental analysis. The results of the elemental analyses for each of the elements show that there is little or no material being lost from feed to product. The errors in the elemental analysis measurements are ± 0.005 for the carbon, hydrogen, and sulfur and ± 0.0005 for the nitrogen.

4.1.3 Feed and Product Distillate Fraction Content

Table 4.3 gives the mass fraction distribution of the distillate fractions of the feed and products.

Because Athabasca bitumen is an extra-heavy feed, there was no gas or naphtha

Table 4.3: Feed and Product Distillate Fraction Content

	Mass Fractions			
Run	Gas	Naphtha	Gas Oil	Residue
Feed	0	0	0.462	0.538
3	0.019	0.024	0.496	0.462
2	0.027	0.032	0.518	0.423
7	0.037	0.031	0.522	0.409
4	0.054	0.037	0.516	0.393
6	0.055	0.052	0.515	0.379
5	0.061	0.045	0.523	0.372
8	0.066	0.051	0.531	0.352
9	0.090	0.046	0.531	0.332

present in the feed. A general trend of increasing gas, naphtha, and gas oil yields and decreasing residue yield with increasing process severity is evident from Table 4.3.

4.1.4 Feed and Product Pseudo-Component Content

Table 4.4 gives the distribution of the pseudo-components of the feed and product runs.

Table 4.4: Feed and Product SARA Fraction (Pseudo-Component) Content

	Mass Fractions						
Run	Gas	N	GO-S	GO-A+P	R-S	R-A+P	R-As
Feed	0	0	0.186	0.276	0.031	0.338	0.170
3	0.019	0.024	0.172	0.324	0.031	0.282	0.149
2	0.027	0.032	0.192	0.327	0.033	0.259	0.131
7	0.037	0.031	0.177	0.345	0.021	0.231	0.157
4	0.054	0.037	0.193	0.323	0.020	0.229	0.145
6	0.055	0.052	0.184	0.330	0.021	0.192	0.166
5	0.061	0.045	0.178	0.345	0.016	0.173	0.183
8	0.066	0.051	0.188	0.342	0.017	0.176	0.159
9	0.090	0.046	0.196	0.335	0.013	0.143	0.177

No noticeable trend is evident in the gas oil pseudo-component yields while the

R-S and R-A+P pseudo-component yields are generally decreasing with increasing severity. The yield of the R-As pseudo-component seems to change less with increasing severity. The fact that the GO-S and GO-A+P pseudo-component yields seem fairly constant while the R-S and R-A+P yields decrease and the gas and naphtha yields increase are indicative of the thermal chemistry that is occurring.

4.1.5 Toluene Insolubles Content

Figure 4.1 gives the toluene insolubles (coke) content of the feed and product runs. The coke content of the feed is 0.38 wt% and corresponds to a severity index value of zero on Figure 4.1.

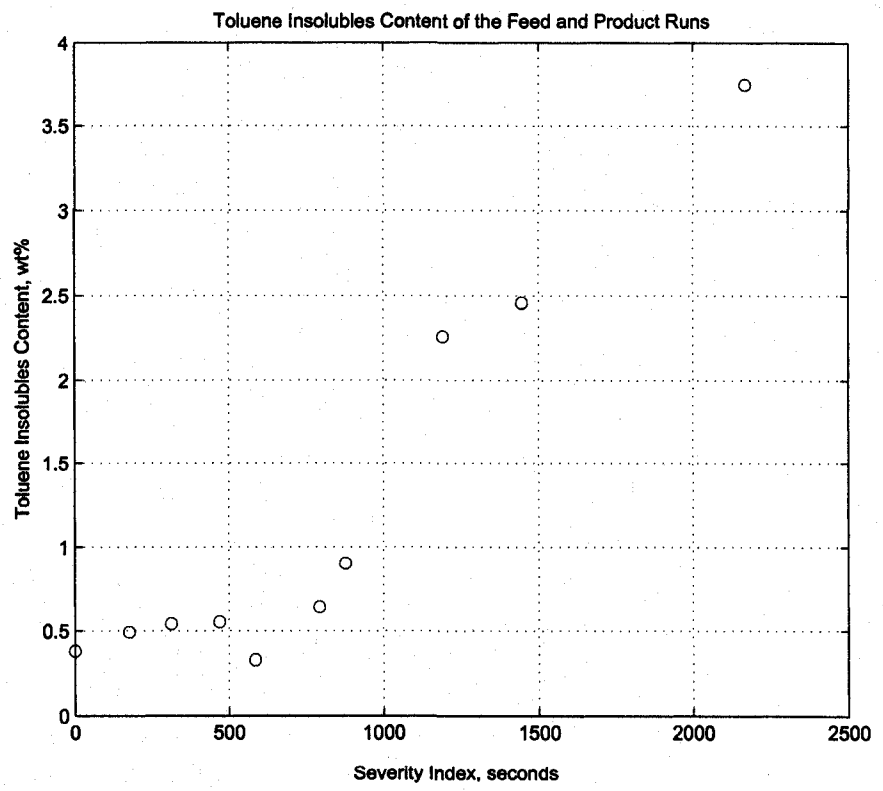

Figure 4.1: Feed and Product Coke Yields

It appears that significant coking does not occur except in Runs 5, 8, and 9 which correspond to severities of 1190, 1450, and 2170 seconds, respectively.

4.1.6 Product Gas Yields

As previously mentioned, carbon type analyses were not performed on the product gases. Instead, the product gases were analyzed for individual components. Table 4.5 gives the normalized yields (moles formed per kg/h of feed) of each of the gases formed in the product runs.

Table 4.5: Product Gas Yields

Run	Feed (kg/h)	Moles Methane	Moles C_2	Moles C_3+	Moles H_2S
3	3	0.154	0.067	0.130	0.153
2	2	0.242	0.107	0.174	0.230
7	3	0.257	0.122	0.302	0.245
4	3	0.505	0.235	0.422	0.337
6	2	0.472	0.224	0.437	0.346
5	2	0.582	0.274	0.486	0.364
8	3	0.473	0.240	0.581	0.344
9	2	0.780	0.392	0.787	0.480

The product gases show a trend of increasing yields with increasing severity. A complete list of the product gases can be found in Appendix B.

4.1.7 NMR Carbon Type Analyses

NMR carbon type analyses were performed on the feed and products. The distribution of some carbon types in the feedstock and one of the product runs, Run 4, is shown in Figure 4.2.

As shown in Figure 4.2, there is an increase in the overall amount of aromatic carbon from feed to product. This indicates that dehydrogenation of cycloparaffinic rings is occurring. Increases in the amount of cycloparaffinic and chain midsection

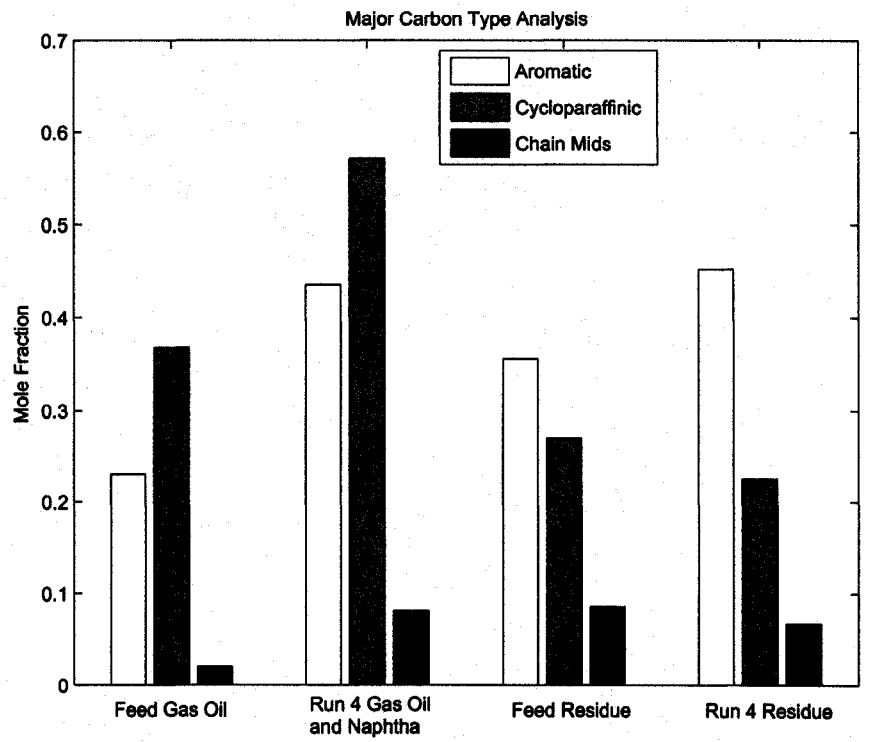

Figure 4.2: Feedstock and Product Carbon Type Analysis

carbon in the gas oil and naphtha fractions are also observed along with decreases in the amount of cycloparaffinic and chain midsection carbon in the residue fraction. As previously discussed, the loss of chain midsection carbon in the residue fraction from feed to product is an indication that thermal cracking has occurred.

Chapter 5

Model Development

An introduction and review of pertinent background topics taken from the literature was given in Chapter 2. A description of the experimental methods and conditions was given in Chapter 3. In this chapter, the two parts of the model are introduced and described. The model was developed using the information about model compounds and bond behaviour taken from literature as well as the data from the NMR carbon type analyses.

5.1 Validation of Conversion Pathways

In studying the chemistry of visbreaking, it is important to determine how the light end products such as the gas phase and naphtha are formed. By combining the information from NMR carbon type analyses with information about the behaviour of the important bond types identified from the model compounds, pathways to predict these product yields have been formulated. Since oil is complex, it is impossible to predict exactly which bonds will break during thermal cracking, so predicting the types of bonds that are likely to break is a way to simplify the problem.

For the mild thermal conditions present during visbreaking, it was assumed that no more than 1 bond per molecule was being broken. It was also assumed that any products formed did not undergo further cracking. In other words, no chain

reactions were assumed to have taken place.

Pathways are described that form the following products:

1. Gas products including methane, C_2, C_3+, and H_2S. The C_2 gases consist of ethane and ethene. The C_3+ gases consists of all gases that are larger than and including propane up to C_5.

2. The naphtha product including cycloparaffin, paraffin, and aromatic carbons. The naphtha aromatic carbon pathway also includes the gas oil aromatic carbon.

Pathways were developed for the light end products (gas and naphtha) because they were new products formed that were not present in the feedstock. As well, a pathway to describe the addition of aromatic carbon in the R-As was developed.

The pathways were proposed and validated by performing conservation of carbon species calculations. The distillate fraction yields and compositions were determined by correlation with severity index.

5.1.1 Gas Formation

Within the gas phase, the products included methane, C_2, C_3+, and H_2S.

Methane Formation

One of the major gas phase products from visbreaking is methane. It made up approximately 25% to 30% of the total gas phase products. Since methane is a small molecule, one might believe that it would have many possible sources. However, the possible sources were narrowed down to only three: methyl-aromatics in the R-A+P and R-As pseudo-components, ethyl-aromatics in the gas oil and R-S pseudo-components, and all methyl-cycloparaffins. The reason for eliminating so many other possibilities lies in the behaviour of model compounds under thermal

cracking conditions. As previously shown, long chain alkyl-substituted aromatics and cycloparaffins tend to release the long chains intact. For shorter chains, this is also the case [13], [46], [47].

The results illustrating the conservation of methyls in the feed and products are shown in Table 5.1. In Table 5.1, the numbers in the row named Feed are the normalized (with feed flow rate) sum of the total moles of methyl species in the feed pseudo-components over the entire run length specified above from the description of the pathway. The numbers in the row named Product are the normalized sum of the moles of methyl species+methane formed over the entire run length. Thus, the total moles of the methyl species in the feed and the total moles of the methyl species+methane in the product were each summed and divided by the feed flow rate for each run to obtain the values under Feed and Product in Table 5.1, respectively. This was done because of the different feed flow rates used in this study. This method was repeated for each subsequent reaction pathway.

Table 5.1: Conservation of Methyl Species in Feed and Product Runs (Normalized)

	Run 3	Run 2	Run 7	Run 4	Run 6	Run 5	Run 8	Run 9
Feed	3.32	3.32	3.32	3.32	3.32	3.32	3.32	3.32
Product	3.40	3.29	3.45	3.31	3.66	3.51	3.69	3.85
% Diff.	-2.4	+0.9	-3.8	+0.3	-9.7	-5.6	-10.6	-14.8

It seems that Runs 8 and 9 have the highest difference with both over 10%. Runs 8 and 9 are the most severe runs so it is likely that bonds other than the ones suggested are breaking to form methane. The low differences for the other runs suggest that the possible sources listed are reasonable for the range of severities.

The equation used for the calculation of percent difference is:

$$\text{Difference} = 2\left\|\frac{(x-y)}{y}\right\| \tag{5.1}$$

where

$$\text{x} = \text{moles of feed source carbon} \tag{5.2}$$

$$y = \frac{\text{Feed Carbon} + \text{Product Carbon}}{2} \tag{5.3}$$

Simplifying equation 5.1 gives:

$$\text{Difference} = 2\left\| \frac{\text{Feed Carbon - Product Carbon}}{\text{Feed Carbon} + \text{Product Carbon}} \right\| \tag{5.4}$$

This method of calculating percent difference is based on how the individual feed and product values compare to the average of the feed and product values.

C_2 Formation

A smaller portion of the gas phase products was ethane and ethene. These two account for 10% to 15% of the total gas phase products. Between the two, ethane is by far the predominant species. The sources of ethane and ethene are similar to those of methane except that each source has an extra carbon on the chain ends. Thus, the likely sources of ethane and ethene are ethyl-aromatics from R-A+P and R-As, propyl-aromatics from the gas oil and R-S pseudo-components, and the ethyl-cycloparaffins.

The results of the conservation of ethyl species in the feed and products are shown in Table 5.2.

Table 5.2: Conservation of Ethyl Species in the Feed and Product Runs (Normalized)

	Run 3	Run 2	Run 7	Run 4	Run 6	Run 5	Run 8	Run 9
Feed	2.97	2.97	2.97	2.97	2.97	2.97	2.97	2.97
Product	2.96	3.03	2.81	2.99	3.31	2.92	3.11	3.25
% Diff.	+0.3	-2.0	+5.5	-0.7	-10.8	+1.7	-4.6	-9.0

The differences for formation of C_2 gas are small and only Run 6 has a difference greater than 10%.

C_3+ Formation

The C_3+ gases range from propane up to the C_5 species. These gases were grouped together because after propane, there were many gases such as butanes and pentanes whose yields were very small and NMR carbon type analysis cannot distinguish butyl+ species. Overall, this group of gases accounts for between 15% and 30% of the total gas products. Propane makes up about half of this group of gases. The logic for the formation of these gases follows that of methane and C_2. This means that all the alkyl-substituted cycloparaffins quantified with α to cycloparaffin species and propyl-aromatics in the R-A+P and R-As are among the likely sources of the C_3+ gases. Also included are the alkyl-substituted aromatics measured as $\alpha\beta$ to aromatics from the GO-S, GO-A+P, and R-S.

The results for the conservation of C_3+ species in the feed and products are shown in Table 5.3.

Table 5.3: Conservation of C_3+ Species in the Feed and Product Runs (Normalized)

	Run 3	Run 2	Run 7	Run 4	Run 6	Run 5	Run 8	Run 9
Feed	6.10	6.10	6.10	6.10	6.10	6.10	6.10	6.10
Product	5.96	5.19	5.37	5.65	5.24	5.44	5.05	4.73
% Diff.	+2.3	+16.1	+12.7	+7.7	+15.2	+11.4	+18.8	+25.3

The maximum difference for the formation of C_3+ gases is in Run 9 at 25.3%. Compared to the differences from the methane and C_2 formation mechanisms, the differences for C_3+ formation are noticeably higher. This likely is due to the fact that not all the $\alpha\beta$-aromatic and α-cycloparaffinic bonds were part of chains that were short enough to form the C_3+ gases. Unfortunately, determining the distribution of specific lengths of paraffinic chains was not possible.

H_2S Formation

The other major product in the gas phase is H_2S. It constitutes approximately 20% to 30% of the gas phase products. However, as gas yields were relatively small, errors in sulfur analyses rendered quantification of sulfur gases from fractions not meaningful. Thus, it was assumed the amount of sulfur lost from each pseudo-component was the same. The amount of sulfur lost in each pseudo-component was determined by measuring the amount of H_2S formed and dividing that by the number of pseudo-components with sulfur in them. Since the stoichiometry of H_2S formation is one-to-one, 1 mole of H_2S formed means that 1 mole of sulfur was lost from the feedstock.

5.1.2 Naphtha Formation

Along with the gas phase, naphtha was formed during visbreaking. Within the naphtha, 3 major carbon types were formed: cycloparaffin, paraffin, and aromatic carbon. Branched paraffinic carbon was included with the naphtha paraffin carbon as its content was small. The conservation of the naphtha aromatic carbon also includes the gas oil aromatic carbon as well.

Cycloparaffin Carbon Formation in Naphtha

Since cycloparaffin carbon is a saturated carbon, its most likely sources would be the saturate pseudo-components, GO-S and R-S. It was also assumed that no cycloparaffin carbons in the GO-S or R-S were lost to dehydrogenation into aromatic rings. Dehydrogenation is most likely to occur when a cycloparaffin ring is in close proximity to an aromatic ring and not on its own under mild visbreaking conditions as previously discussed.

The results of the conservation of cycloparaffin species in the feed and products are shown in Table 5.4.

Table 5.4: Conservation of Cycloparaffinic Species in the Feed and Product Runs (Normalized)

	Run 3	Run 2	Run 7	Run 4	Run 6	Run 5	Run 8	Run 9
Feed	8.06	8.06	8.06	8.06	8.06	8.06	8.06	8.06
Product	7.56	7.56	6.93	7.57	7.00	6.63	7.55	6.83
% Diff.	+6.4	+6.4	+15.1	+6.3	+14.1	+19.5	+6.5	+16.5

The trend for the differences for this pathway seems to be either around 6% or above 14%. It is possible that some of the cycloparaffins from the GO-S and R-S are large enough that they would end up in the gas oil fraction instead of the naphtha after cracking.

Paraffin Carbon Formation in Naphtha

The paraffinic carbon formed in the naphtha has many possible sources. Most of the paraffin carbon in the feedstock is attached to either an aromatic ring or cycloparaffin ring. Branched paraffinic carbon was also included as well. After analyzing the NMR data, the average chain lengths in the R-As pseudo-component were too short to generate paraffin chains that would end up in the naphtha, so the R-As was eliminated as a significant source of paraffin carbon in naphtha.

The results of the conservation of paraffin carbon species in the feed and products are shown in Table 5.5.

Table 5.5: Conservation of the Paraffinic Species in the Feed and Product Runs (Normalized)

	Run 3	Run 2	Run 7	Run 4	Run 6	Run 5	Run 8	Run 9
Feed	10.74	10.74	10.74	10.74	10.74	10.74	10.74	10.74
Product	11.32	12.70	10.71	10.73	10.77	10.17	10.52	9.57
% Diff.	-5.3	-16.7	+0.3	+0.1	-0.3	+5.5	+2.1	+11.5

The difference for paraffin formation in the naphtha fraction are excellent and indicate good agreement except for Run 2 and Run 9. This supports the hypothe-

sis that paraffinic carbon in the naphtha can come from every pseudo-component except for the R-As.

Aromatic Carbon Formation in Naphtha and Gas Oil

The final reaction pathway for naphtha is that of the aromatic carbon. This pathway also includes the gas oil aromatic carbon. Since the average aromatic cluster size for naphtha and gas oil are approximately 1 and 2 rings, respectively, the only possible sources for this are the GO-A+P and R-A+P pseudo-components, having average aromatic cluster sizes of 1 and 2, respectively. The R-As pseudo-component has an average aromatic cluster size of 4 aromatic rings so it is not likely to be a significant source of 1 and 2-ring aromatics found in the naphtha and gas oil.

The results of the conservation of aromatic carbon species in the feed and product are shown in Table 5.6. The loss of cycloparaffinic carbon in the GO-A+P and R-A+P pseudo-components were subtracted from the product total so that they could be taken into account in the balance.

Table 5.6: Conservation of Aromatic Carbon Species in the Feed and Product Runs (Normalized)

	Run 3	Run 2	Run 7	Run 4	Run 6	Run 5	Run 8	Run 9
Feed	14.93	14.93	14.93	14.93	14.93	14.93	14.93	14.93
Product	18.18	16.81	19.28	18.81	15.96	16.79	18.14	16.80
% Diff.	-19.6	-11.8	-25.4	-23.0	-6.7	-11.7	-19.4	-11.8

For the formation of aromatic carbon in the naphtha fraction, the differences are much more significant with the lowest being 6.7%. One possible reason for the higher differences here is that in the carbon type analysis for the product runs, aromatic carbon formation was greater than the loss of cycloparaffins. This is not possible unless there are aromatization reactions happening. Aromatization reactions are not likely unless proper catalysts and conditions are present [17]. The differences

may be indicating that there is some contribution from the R-As pseudo-component as well.

5.1.3 Residue Formation

Aromatic Carbon Formation in R-As

Finally, the last pathway follows changes in aromatic carbon content in R-As. From the NMR carbon type analyses, an increase in aromatic carbon in the R-As pseudo-component was observed. Here, the assumption of no aromatization of chains still applies. The sources for formation of new R-As aromatic species are R-A+P and dehydrogenation of cycloparaffin rings in R-As. Polyaromatic species with 3 or 4 rings with paraffin chains attached are soluble in pentane. After thermal cracking, 1 or more chains could be removed causing the polyaromatic species remaining to be insoluble in pentane and end up in the R-As pseudo-component. Similarly, the dehydrogenation of multi-ring hydroaromatic species could result in the molecule no longer being soluble in pentane.

The results for the R-As aromatic carbon formation balances are shown in Table 5.7.

Table 5.7: R-As Aromatic Addition Balances (Normalized)

	Run 3	Run 2	Run 7	Run 4	Run 6	Run 5	Run 8	Run 9
Feed	13.20	13.20	13.20	13.20	13.20	13.20	13.20	13.20
Product	12.99	11.38	13.16	12.53	12.09	12.65	12.17	12.13
% Diff.	+1.6	+14.8	+0.3	+5.2	+8.8	+4.3	+8.1	+8.4

The differences for the addition of aromatic carbon in R-As are very good except for Run 2. This supports the hypothesis that the increase of aromatic carbon in R-As is due to the dehydrogenation of cycloparaffin rings and migration from R-A+P.

From the reaction pathways, it seems that the R-A+P pseudo-component is a significant source of distillate product while the R-As pseudo-component contributes little.

5.2 Product Yield Correlations

Severity index has proven to be a useful tool to correlate and predict product yields from thermal cracking [39]. In this work, severity index was found to correlate with the yields of the distillate fractions, individual gas yields, as well as yields of major carbon types within the liquid distillate fractions and coke formation (toluene insolubles). The complete list of severity index correlations is given in Table 5.8.

Table 5.8: Summary of Severity Index Correlations

Distillate Fraction	Product Yields Correlated
Gas	Methane, C_2, C_3+, H_2S
Naphtha	Cycloparaffinic, Paraffinic, Aromatic Carbon
Gas Oil	Cycloparaffinic, Aromatic, Chain-Midsection Carbon
Residue	Cycloparaffinic, Paraffinic, Branch-Paraffinic, Aromatic, Chain-Midsection Carbon, $\alpha\beta$-Aromatic Carbon Coke Formation

5.2.1 Gas Yields

In the gas product, the overall yield as well as the yields of methane, C_2, C_3+, and H_2S were correlated with severity index. Figure 5.1 shows the correlation of the overall gas yield with severity index. As expected, the gas yields increase with severity.

The dashed lines in Figure 5.1 indicate prediction errors while the error bars in Figure 5.1 indicate data measurement error. Both of these error types will be discussed later.

In Figure 5.1, it is clear that there are two distinct trend lines. The trend line on the left (low severity region) is where little coking is present while the trend line on the right (high severity region) is where coking has begun (2-3%) as shown in

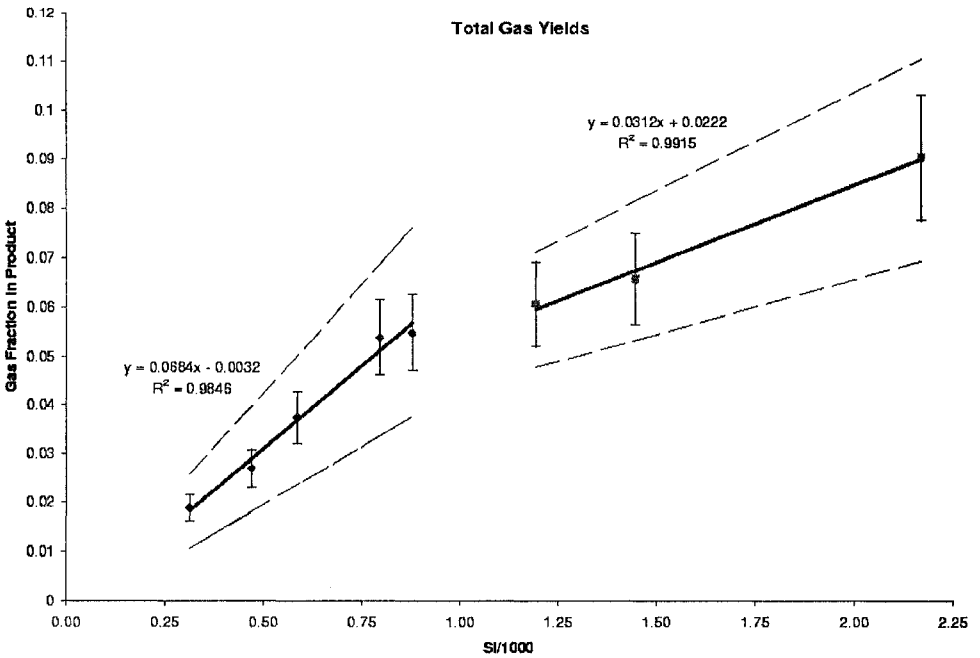

Figure 5.1: Correlation of Overall Gas Yield with Severity Index

Figure 4.1. The dividing line between the two regions seems to be around where SI/1000 (reduced severity) is approximately equal to 1.

In Figure 5.2, the correlation of methane formation with reduced severity is shown where the quantity plotted on the y-axis is normalized methane. Much like the normalized conservation calculations for the conversion pathways discussed previously, normalized methane is defined as the moles of methane produced in each run divided by the mass flow rate of the feed in kg/h for that run. Similarly, normalized yields for C_2, C_3+, and H_2S were correlated with reduced severity as well and are listed in Table 5.9. The plots of the C_2, C_3+, and H_2S yield correlations can be found in Appendix C.

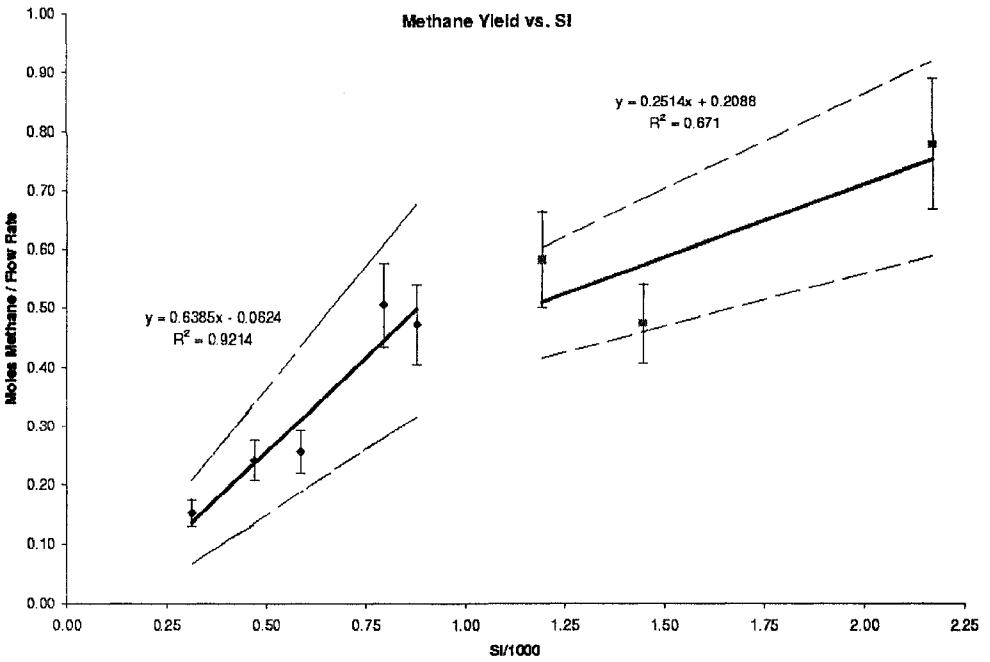

Figure 5.2: Correlation of Methane Yield with Severity Index

5.2.2 Naphtha Yields

The overall naphtha fraction yield and the yield of aromatic, cycloparaffinic, and paraffinic carbon in the naphtha were correlated with severity index. The overall naphtha fraction yield correlation is shown in Figure 5.3.

The naphtha carbon type yield correlations are similar to the individual gas yield correlations in that the correlations are for normalized carbon types. Thus, the cy-

Table 5.9: Normalized C_2, C_3+, and H_2S (Moles Formed per kg/h Feed) Yield Correlations

Gas	Low Severity Region	R^2	High Severity Region	R^2
C_2	0.2877SI - 0.0214	0.94	0.141SI + 0.0758	0.80
C_3+	0.5675SI - 0.0496	0.97	0.3031SI + 0.1323	0.99
H_2S	0.3366SI + 0.0581	0.98	0.1336SI + 0.1813	0.86

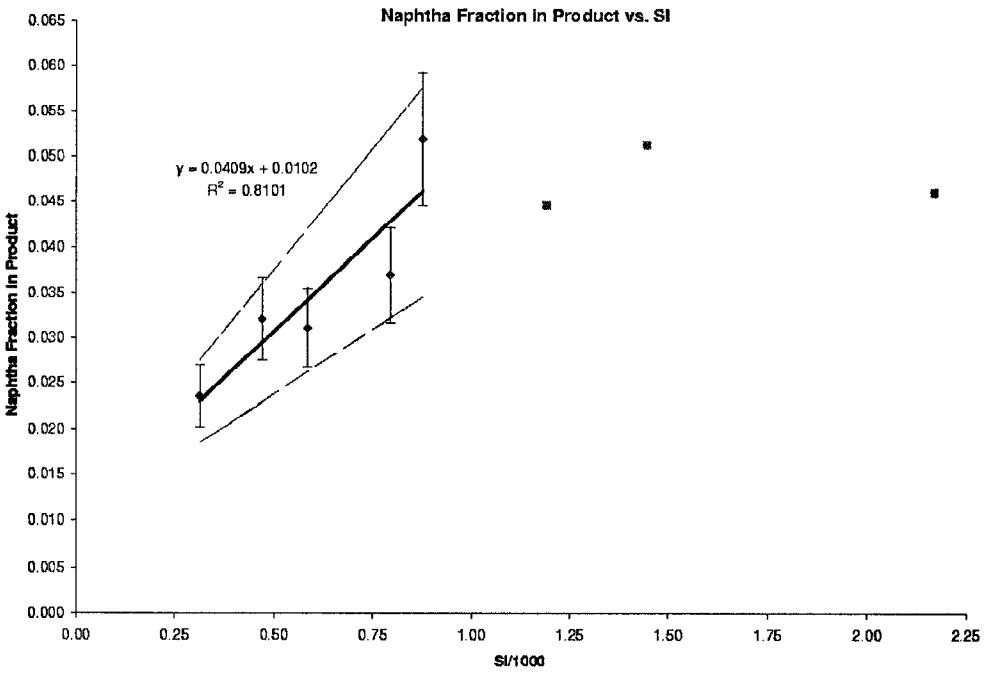

Figure 5.3: Correlation of Overall Naphtha Yields with Severity Index

cloparaffinic, paraffinic, and aromatic carbon yield correlations are for moles of each carbon type formed per kg/h of feed. The naphtha carbon type yield correlations are listed in Table 5.10. The plots of the naphtha carbon type yield correlations can be found in Appendix C.

Table 5.10: Normalized Naphtha Carbon Type Yield (Moles per kg/h Feed) Correlations

Carbon Type	Low Severity Region	R^2
Cycloparaffin	0.7399SI + 0.1811	0.95
Paraffin	0.5257SI + 0.1296	0.75
Aromatic	0.3838SI + 0.1144	0.79

The data for naphtha in the high severity region was not correlated. There was no strong trend as either the slopes or correlation coefficients (R^2) were close to zero for all carbon types. Thus, an average value was each taken for the cycloparaffinic,

paraffinic, and aromatic carbon yields as well as the overall naphtha yield. Those values are summarized in Table 5.11.

Table 5.11: Summary of Normalized Naphtha Carbon Yields (Moles Formed per kg/h Feed) in High Severity Region

Product	Normalized Yield Value
Naphtha	0.0473
Cycloparaffin	0.8139
Paraffin	0.6261
Aromatic	0.4461

5.2.3 Gas Oil Yields

As gas oil was present in the feed, the gain or loss of carbon types relative to that present in the feed was determined. It was found that aromatic and chain midsection carbon yields in the gas oil fraction were correlated with reduced severity. As the yields of the gas, naphtha, and residue were determined independently, the yields of gas oil was calculated by difference as shown by equation 5.5.

$$\text{Gas Oil Fraction} = 1 - \text{Residue Fraction} - \text{Naphtha Fraction} - \text{Gas Fraction} \quad (5.5)$$

The chain midsections yield correlation is shown in Figure 5.4.

In Figure 5.4, a gain of chain midsection carbon in the gas oil while a loss of chain midsection carbon in the residue is observed. This is an indication that much of the residue is being converted into gas oil. The rest of the residue that was converted ended up as gas and naphtha.

Cycloparaffinic carbon yield did not show a strong trend and so an average value for the fraction of cycloparaffins lost in the gas oil was used for both the low severity and high severity regions. The correlations for the aromatic and cycloparaffin yields are listed in Table 5.12. The plot of the gas oil aromatic carbon yield correlation can be found in Appendix C.

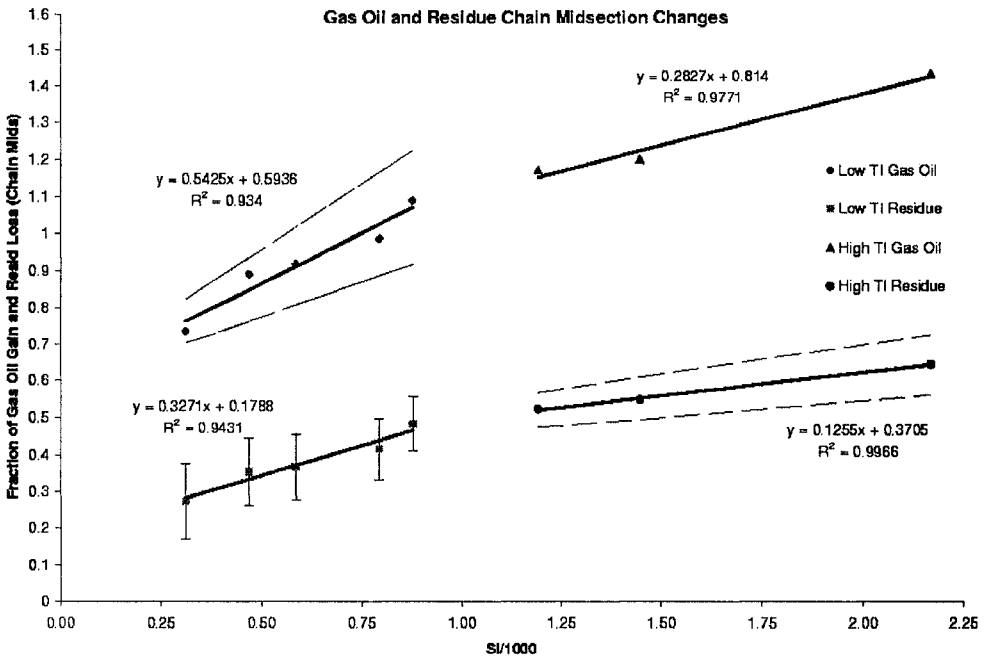

Figure 5.4: Gas Oil and Residue Chain Midsection Yield Correlation with Severity Index

Table 5.12: Gas Oil Carbon Type Yield Correlations

Carbon Type	Low Severity Region	R^2	High Severity Region	R^2
Cycloparaffin	0.1521	-	0.1521	-
Aromatic	0.247SI + 0.2963	0.66	0.118SI + 0.4255	0.85

5.2.4 Residue Yields

The overall residue fraction yield as well the loss of cycloparaffinic, aromatic, paraffinic, branch-paraffinic, chain midsection, and $\alpha\beta$-aromatic carbon types were correlated with severity index. The overall residue fraction yield correlation is shown in Figure 5.5. The correlation for chain midsection yield in the residue fraction is shown with the gas oil chain midsection correlations on Figure 5.4.

The fraction of carbon types lost in the residue was correlated with severity index. Aromatic carbon yield did not show a strong trend and so an average value

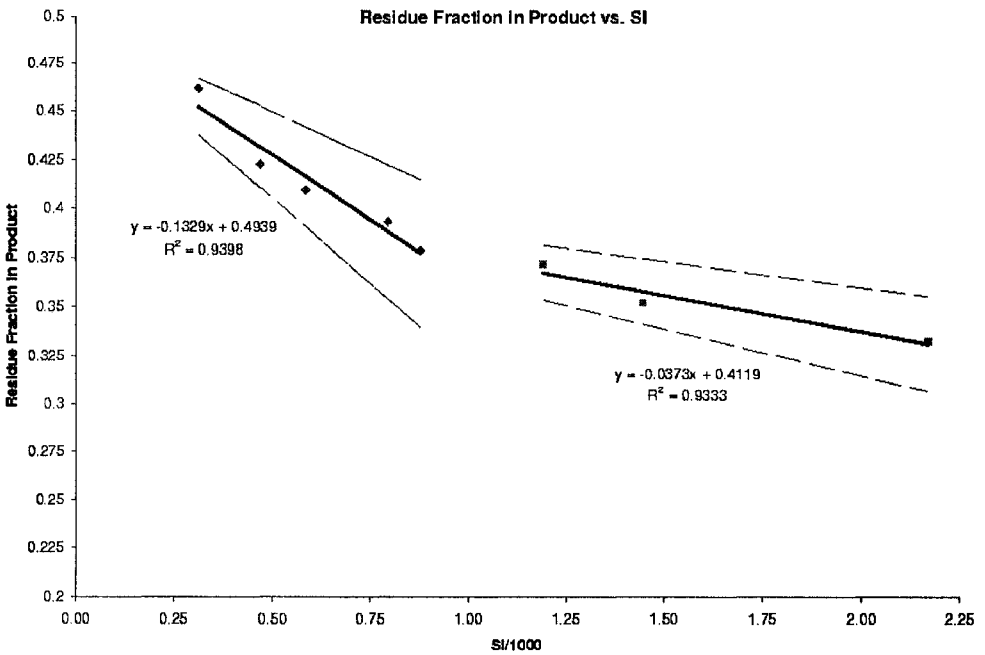

Figure 5.5: Correlation of Overall Residue Yields with Severity Index

for the fraction of aromatics gained in the residue was used for the low and high severity regions. The correlations for the other carbon types are listed in Table 5.13. The plots of the carbon type yield correlations from Table 5.13 can be found in Appendix C.

Table 5.13: Residue Carbon Type Yield Correlations

Carbon Type	Low Severity Region	R^2	High Severity Region	R^2
Cycloparaffin	0.4424SI + 0.069	0.87	0.1403SI + 0.339	0.94
Aromatic	0.0356	-	0.0356	-
Paraffin	0.3904SI + 0.1514	0.94	0.082SI + 0.4509	0.99
Branch-Paraffin	0.5158SI + 0.097	0.69	0.0838SI + 0.4863	0.94
$\alpha\beta$-Aromatic	0.4411SI + 0.0527	0.85	0.1775SI + 0.2127	0.99

5.2.5 Coke Yields

When comparing the coke yields, as measured by toluene insolubles content, of the feed with those of the product runs (Figure 4.1), only runs 5, 8, and 9 have significant coking. The coke yields from runs 5, 8, and 9 were correlated with severity index and is shown in Figure 5.6. The coke yields from the runs in the low severity region were averaged to a value of 0.58 wt%.

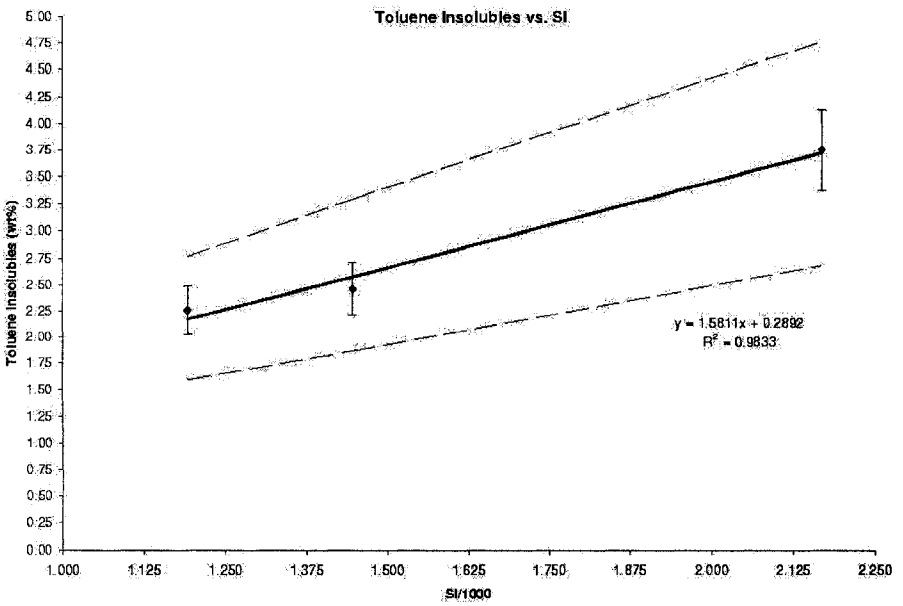

Figure 5.6: Correlation of Toluene Insolubles Content with Severity Index

Increasing severity is likely resulting in increasing cleavage of side chains from the polyaromatic species in the residue. That coke formation (measured as toluene insolubles) does not begin to increase until a reduced severity of 1 may indicate that multiple cleavage of chains from polyaromatic species is beginning to occur at this point. The resulting polyaromatic species with no chains attached would no longer be soluble in toluene and so would contribute to the coke yield.

Interestingly, the trends evident in many of the severity index correlation plots

are similar to that of DDP conversion (Figure 2.24) in that conversion seems to be reaching a maximum. This could indicate that, under these conditions, the large pol-yaromatic species are mainly responsible for Athabasca bitumen conversion where the oil is reaching a maximum conversion because of a lack of feed to convert.

Chapter 6

Model Use and Validation

6.1 Prediction of Product Composition

One of the reasons for developing a model is to be able to predict product yields. The steps to use the model are outlined below. An example is given in Appendix D. For a particular reduced severity (SI/1000), the overall gas phase, naphtha, and residue fraction yields can be estimated from the correlations from Figures 5.1, 5.3, and 5.5, respectively. As the distillate fraction yields are mass fractions, the overall gas oil fraction yield can be calculated by difference from the gas phase, naphtha, and residue fraction yields from equation 5.5.

Next, the yields of the individual gases in the gas phase are estimated. To estimate the moles of each gas formed, the following equation is used:

$$\text{Moles of Each Gas} = \text{Feed Flow Rate} * \left(\frac{\text{Moles Gas Formed}}{\text{Feed Flow Rate}} \right) \tag{6.1}$$

The value of (Moles Gas Formed/Feed Flow Rate) is obtained for each species from its respective severity index correlation (Table 5.9).

In the naphtha fraction, the yields of aromatic, cycloparaffinic, and paraffinic carbon can be estimated. The carbon type yields in the naphtha are estimated in a similar manner as the individual gases:

$$\text{Moles Carbon} = \text{Feed Flow Rate} * \left(\frac{\text{Moles Carbon Formed}}{\text{Feed Flow Rate}} \right) \tag{6.2}$$

Similarly, the carbon type yields in the gas oil and residue fraction are estimated. In order to use the correlations to determine the yield each carbon type in the gas oil and residue pseudo-components, the following equation is used:

$$\text{Product Carbon Type} = \text{Feed Carbon Type} * (1 \pm \text{Fraction Gained/Lost}) \quad (6.3)$$

Finally, the coke yield is estimated. If the reduced severity is less than 1, then the average value of toluene insolubles content in the low severity region (0.58 wt%) is used. If the reduced severity is greater than 1, then the correlation from Figure 5.6 is used to estimate the toluene insolubles content.

6.2 Validation of Method

Since no data from other oils was available, the method of using severity index to correlate the yields of the distillate fractions and the various carbon types within those fractions was validated by removing one run from the data set, re-estimating the correlations and predicting the data from the removed run. The data from the removed run was predicted using the re-estimated equations and compared to the actual data. First, the data from Run 2 was removed and all of the correlations listed above were re-estimated. Then, the yields from Run 2 were estimated. The average error was calculated to be approximately 8.2%. Next, the data from Run 2 was put back in and the data from Run 4 was removed and the procedure was repeated. The average error was 10.7%. The results are shown in Table 6.1.

This validation method was used because of the relatively few number of data points available. It was not possible to set aside a separate set of data points exclusively for validation because there were only 5 data points in the lower severity region and 3 data points in the higher severity region. A true validation process cannot be achieved with only one feedstock and so a more thorough validation process will take place when the visbreaking of more feedstocks is studied. The inclusion

of more feedstocks will be part of the future work.

The correlations of the yields and severity index were excellent as many of the correlation coefficients (R^2) were above 0.80. Thus, the correlations can be used to predict product yields given the temperature, residence time, and flow rate for Athabasca bitumen.

Table 6.1: Results of Method Validation

	Run 2			Run 4		
Distillate Fraction Masses (Grams)						
	Actual	Predicted	% Error	Actual	Predicted	% Error
Gas	54	59.23	9.7	161.1	148.0	8.1
Naphtha	64.2	60.2	6.2	110.7	136.6	23.3
Gas Oil	1036.6	1015.1	2.1	1548.3	1560.7	0.8
Residue	1179.9	1154.9	2.4	845.19	865.48	2.1
Individual Gas Yields (Moles)						
	Actual	Predicted	% Error	Actual	Predicted	% Error
Methane	0.48	0.50	2.6	1.51	1.22	19.3
C_2	0.21	0.23	6.1	0.71	0.58	18.2
C_3+	0.35	0.43	24.5	1.26	1.17	7.3
H_2S	0.46	0.43	6.1	1.01	0.96	5.1
Naphtha Carbon Yields (Moles)						
	Actual	Predicted	% Error	Actual	Predicted	% Error
Cycloparaffin	1.12	1.06	5.4	2.16	2.39	10.5
Paraffin	0.82	0.59	28.3	1.34	1.80	34.1
Aromatic	0.61	0.75	24.1	1.08	1.35	25.3
Gas Oil Carbon Yields (Moles)						
	Actual	Predicted	% Error	Actual	Predicted	% Error
Cycloparaffin	19.81	20.68	4.4	32.79	30.76	6.2
Aromatic	21.75	21.40	1.6	33.01	34.47	4.4
Chain Mid	2.58	2.52	2.4	4.05	4.18	3.2
Residue Carbon Yields (Moles)						
	Actual	Predicted	% Error	Actual	Predicted	% Error
Cycloparaffin	13.84	14.72	6.4	18.78	17.07	9.1
Aromatic	24.75	25.59	3.4	37.50	38.50	2.7
Paraffin	6.60	6.64	0.5	8.66	8.01	7.5
Branch-Paraffin	2.97	2.49	16.3	2.59	2.89	11.6
Chain Mids	4.18	4.31	3.2	5.67	5.31	6.4
$\alpha\beta$-Aromatic	2.04	2.23	9.3	2.88	2.59	10.2
Coke Yield (wt%)						
	Actual	Predicted	% Error	Actual	Predicted	% Error
Coke	0.54	0.58	7.4	0.64	0.58	9.4

6.3 Error Analysis

6.3.1 Prediction Errors

Two different error analyses were performed. The first was to determine the error bounds for the correlations for the yields in Chapter 5, shown as dashed lines on the correlation plots. All of the correlations have the following form:

$$y = f(SI) \tag{6.4}$$

The error was estimated from the partial derivative of equation 6.4 and is known as the Holman method [48].

$$\frac{\partial y}{\partial SI} = \frac{dy}{dSI}\Delta SI \tag{6.5}$$

$$\Delta SI = \sqrt{\left(\frac{\partial SI}{\partial E_A}\Delta E_A\right)^2 + \left(\frac{\partial SI}{\partial \tau}\Delta\tau\right)^2 + \left(\frac{\partial SI}{\partial T}\Delta T\right)^2} \tag{6.6}$$

For equation 6.6, ΔE_A = 5000 cal/mol, $\Delta\tau$ = 2 min (120 seconds), and ΔT = 5 K. Thus, the upper and lower bounds of the yield estimates from the correlations can be calculated. When using the yield correlations to estimate the yields of visbreaking, the actual yields are likely to fall within the upper and lower bounds.

6.3.2 Measurement Errors

The second type of error analysis performed was a form of measurement error. This is what is represented by the error bars that are on some of the correlation plots. On the y-axis, the quantities have one of two different forms:

$$y = \frac{a}{b} \tag{6.7}$$

$$y = 1 - \frac{b}{a} \tag{6.8}$$

Table 6.2: Measurement Error Summary

Y-Axis Quantity	a	b
Distillate Frac. Yield	Distillate Frac. Mass	Total Product Mass
Individual Gas Yield	Moles of Gas	Feed Flow Rate
Frac. C Type Gained/Lost	Moles C Type-Feed	Moles C Type-Product

For the distillate fraction yield and individual gas yield correlations, equation 6.7 applies and for the fraction of carbon types gained or lost, equation 6.8 applies. A summary of the a and b variables is given in Table 6.2.

The individual error for each quantity of a and b was taken to be 10% of its value. For example, if the moles of methane formed in Run 2 was 0.5 moles, the methane error would be 0.05 moles. If the feed flow rate was 2 kg/h, the error would be 0.2 kg/h. Just like for the severity index correlations, the error for equations 6.7 and 6.8 were obtained using the Holman method [48]. The errors for equations 6.7 and 6.8 are shown by equations 6.9 and 6.10, respectively.

$$Error = \sqrt{\left(\frac{\Delta a}{b}\right)^2 + \left(\frac{a}{b^2}\Delta b\right)^2} \tag{6.9}$$

$$Error = \sqrt{\left(\frac{b}{a^2}\Delta a\right)^2 + \left(\frac{\Delta b}{a}\right)^2} \tag{6.10}$$

6.4 Comparison to Other Model Approaches

As previously mentioned, the loss of certain bond types indicates that thermal cracking is occuring. This is shown by the loss of cycloparaffinic carbon and a gain in aromatic carbon, the loss of $\alpha\beta$-aromatic carbon in the residue fraction as well as a loss of chain midsection carbons in the residue fraction and a gain of chain midsection carbons in the gas oil fraction. With the severity index correlations, the yields of visbreaking runs on Athabasca bitumen can be estimated. All that is needed is the visbreaking temperature in Kelvin, the residence time in seconds, and

the feed flow rate in kg/h. If the reduced severity (SI/1000) is less than 1, then the low severity region correlations are used for predicting, and if the reduced severity is greater than 1, then the high severity region correlations are used for predicting.

The model presented in this work is different than other models presented previously because:

1. It is able to predict yields of carbon types which will be useful for correlating product quality with visbreaking conversion.

2. Specific reaction pathways for the formation of light end (gas and naphtha) products from visbreaking are proposed and validated. This gives an increased level of understanding of the thermal chemistry occurring during visbreaking.

Both of the above were achieved without the need to estimate kinetic parameters. As the correlations developed are based on fundamental chemical principles, it is possible that the model approach will be transferable to other feedstocks.

Overall, the form of the model is very simple. Reaction chemistry pathways and the prediction of product yields with severity index do not require extensive or difficult calculations. Considering the success in describing visbreaking reaction chemistry and predicting visbreaking yields, the model's simplicity makes it extremely useful.

Chapter 7

Conclusions and Future Work

7.1 Conclusions

In this work, a new form of visbreaking model has been presented. Instead of predicting product yields from a reaction network that included kinetic parameters, reaction pathways were developed to describe the formation of light end products while product yields were correlated with severity index. The reaction mechanisms were developed by utilizing information about bond behaviour from the pyrolysis of model compounds from the literature. Overall, the form of this model is quite different from other models previously proposed. Past models usually involved estimating the kinetic parameters of a reaction network. For this model, no kinetic parameters needed to be estimated. The reaction pathways describe the formation of the light end products well. The errors for the gas phase product formation pathways are lower than the naphtha carbon type formation pathways. This could indicate that there are additional sources of the naphtha carbon types that were not taken into account. Overall, the low percentage differences indicate that the assumptions made were reasonable except for the highest severities. For the highest severities, the assumption that only 1 bond is breaking to form products may not be correct. From the reaction chemistry pathways, it seemed that most of the cracking occurs in the residue fraction, especially the R-A+P pseudo-component while the

R-As contributed less. When examining the model compounds, the aromatic compounds (PDB, UDN, DDP) are more reactive than the cycloparaffinic compounds (TDC, UDD) with DDP being the most reactive. Because DDP is the most reactive, this suggests that Athabasca bitumen conversion under visbreaking conditions is mainly through cleavage of chain species from larger polyaromatic ring species.

The definition of severity index presented by Yan (1990) [42] proved useful for correlating the product yields of visbreaking of Athabasca bitumen. The distillate fraction yields, individual gas yields, carbon type yields, and coke yield were all correlated with severity index. Most of the data correlated well with severity index with most R^2 values greater than 0.80. Nevertheless, severity index can be used to predict yields of the visbreaking of Athabasca bitumen without the need for kinetic parameters.

Overall, reaction pathways were developed and the carbon type yields were found to correlate with severity index because of new information and data that was obtained by the use of NMR spectroscopy and a new method for defining pseudo-components. Previously, this level of detail in the data was not available and so this type of model development was not possible. The reaction pathways developed in this work should contribute to a better understanding of thermal cracking chemistry while the severity index correlations should enable visbreaking yields to be easily estimated.

7.2 Future Work

Future work will focus on testing the transferability of the new method to other feedstocks from around the world. The goal will be to predict visbreaking yields regardless of feedstock source. Relying on carbon bond type information will likely make this an achievable goal because the carbon bonds quantified from NMR spectroscopy will appear in all feedstocks. Only the relative amounts of each carbon

type will vary. With more feedstocks, the reaction chemistry of visbreaking can be investigated and refined further by looking for similarities among feedstocks.

The work presented here is a small step towards a better understanding of thermal cracking processes and thermal chemistry. New information about thermal chemistry has been proposed. The inclusion of more feedstocks will allow for a more thorough validation of the thermal chemistry and yield correlations proposed in this work. Ultimately, it would also be desirable to apply this method to model other thermal cracking processes such as hydroconversion and coking.

Bibliography

[1] V. Simanzhenkov and R. Idem. *Crude Oil Chemistry*. Marcel Dekker Inc., 2003.

[2] *Oil and Gas Journal Databook, 2002 Edition*. Pennwell Corporation, 2002.

[3] G.E. Dolbear, A. Tang, and E.L. Moorehead. Upgrading studies with californian, mexican, and middle eastern heavy oils. In R.H. Filby and J.F. Branthaver, editors, *Metal Complexes in Fossil Fuels: Geochemistry, Characterization, and Processing*, pages 220–232. American Chemical Society, 1987.

[4] M.R. Gray. *Upgrading Petroleum Residues and Heavy Oils*. Marcel Dekker, Inc., 1994.

[5] P. Leprince. *Petroleum Refining. 3. Conversion Processes*. Institut Francais du Petrole, 2001.

[6] J.G. Speight. *Petroleum Refining Processes*. Marcel Dekker Inc., 2002.

[7] M. Hus. Visbreaking process has strong revival. *Oil and Gas J.*, 79:109–120, 1981.

[8] J.H. Gary and G.E. Handwerk. *Petroleum Refining: Technology and Economics, 4th Edition*. Marcel Dekker Inc., 2001.

[9] D.E. Allan, C.H. Martinez, C.C. Eng, and W.J. Barton. Visbreaking gains renewed interest. *Chem. Eng. Prog.*, 79:85–89, 1983.

[10] M. Akbar and H. Geelen. Visbreaking uses soaker drum. *Hydrocarbon Processing*, 60:81–85, 1981.

[11] S.W. Benson. *Thermochemical Kinetics, 2nd Edition*. John Wiley and Sons, 1976.

[12] P.E. Savage and M.T. Klein. Asphaltene reaction pathways. 2. pyrolysis of n-pentadecylbenzene. *Ind. Eng. Chem. Res.*, 26:488–494, 1987.

[13] M.C. Smith and P.E. Savage. Reactions of polycyclic alkylaromatics: Structure and reactivity. *AIChE J.*, 37:1613–1624, 1991.

[14] P.E. Savage, G.E. Jacobs, and M. Javanmardian. Autocatalysis and aryl-alkyl bond cleavage in 1-dodecylpyrene. *Ind. Eng. Chem. Res.*, 28:645–654, 1989.

[15] P.E. Savage and M.T. Klein. Asphaltene reaction pathways. 4. pyrolysis of tridecylcyclohexane and 2-ethyltetralin. *Ind. Eng. Chem. Res.*, 27:1348–1356, 1988.

[16] T.I. Mizan, P.E. Savage, and B. Perry. Pyrolysis of polycyclic perhydroarenes. 2. 1-n-undecylperhydronaphthalene. *Energy and Fuels*, 11:107–115, 1997.

[17] J.D. Hepworth. *Aromatic Chemistry*. Royal Society of Chemistry, 2002.

[18] J.B. Lambert and E.P. Mazzola. *Nuclear Magnetic Resonance Spectroscopy: An Introduction to Principles, Applications, and Experimental Methods*. Pearson Education Inc., 2004.

[19] L. Petrakis and D. Allen. *NMR for Liquid Fossil Fuels*. Elsevier, 1987.

[20] R.B. Williams. Symposium on composition of petroleum oils, determination and evaluation. *ASTM Spec. Tech. Pub.*, 224:168–194, 1958.

[21] J.K. Brown and W.R. Ladner. A study of the hydrogen distribution in coal-like materials by high-resolution nuclear magnetic resonance spectroscopy ii - a comparison with infra-red measurement and the conversion to carbon structure. *Fuel*, 39:87–96, 1960.

[22] S.A. Knight. Analysis of aromatic petroleum fractions by means of absorption mode Carbon-13 N.M.R. spectroscopy. *Chem. Ind.*, pages 1920–1923, 1967.

[23] D.R. Clutter, L. Petrakis, R.L. Stenger, Jr., and R.K. Jensen. Nuclear magnetic resonance spectrometry of petroleum fractions. *Analytical Chem.*, 44:1395–1405, 1972.

[24] M.U. Hasan, M.F. Ali, and A. Bukhari. Structural characterization of Saudi Arabian heavy crude oil by N.M.R. spectroscopy. *Fuel*, 62:518–523, 1983.

[25] A. Majid, J. Bornais, and R.A. Hutchison. Characterization of various bitumen samples from tar sands. *Am. Chem. Soc., Div. Pet. Chem., Preprints*, 33:283–291, 1988.

[26] B.M.L. Bhatia, B.S. Goyal, D.S. Aswal, M.K.S. Aloopwan, and G.C. Kothari. Structural characterization of VGOs from western region crudes by NMR spectroscopy. *Pet. Sci. Tech.*, 21:125–132, 2003.

[27] V. Vishnoi, K.M. Agrawal, I.D. Singh, and B.B. Raizada. Compositional analysis of waxy distillate fractions by ^{1}H and ^{13}C NMR spectroscopy. *Pet. Sci. Tech.*, 23:931–937, 2005.

[28] S. Zhao, Y. Zhou, Z. Xu, C. Xu, and K.H. Chung. A new group contribution method for estimating boiling point of heavy oil. *Pet. Sci. Tech.*, 24:253–263, 2006.

[29] J.M. Sheremata, M.R. Gray, H.R. Dettman, and W.M. McCaffrey. Quantitative molecular representation and sequential optimization of Athabasca asphaltenes. *Energy and Fuels*, 18:1377–1384, 2004.

[30] K. Al-Zaid, Z.H. Khan, A. Hauser, and H. Al-Rabiah. Composition of high boiling petroleum distillates of kuwait crude oils. *Fuel*, 77:453–458, 1998.

[31] F. Ali, Z.H. Khan, and N. Ghaloum. Structural studies of vacuum gas oil distillate fractions of Kuwaiti crude oil by nuclear magnetic resonance. *Energy and Fuels*, 18:1798–1805, 2004.

[32] G. Michael, M. Al-Siri, Z.H. Khan, and F.A. Ali. Differences in average chemical structures of asphaltene fractions separated from feed and product oils of a mild thermal processing reaction. *Energy and Fuels*, 19:1598–1605, 2005.

[33] L. Petrakis, D.T. Allen, G.R. Gavales, and B.C. Gates. Analysis of synthetic fuels for functional group determination. *Analytical Chem.*, 55:1557–1564, 1983.

[34] D.T. Allen, D.W. Grandy, K. Jeong, and L. Petrakis. Heavier fractions of shale oils, heavy crudes, tar sands, and coal liquids: Comparison of structural profiles. *Ind. Eng. Chem. Proc. Des. Dev.*, 24:737–742, 1985.

[35] W.R. Shu and V.N. Venkatesan. Kinetics of thermal visbreaking of a Cold Lake bitumen. *J. Can. Pet. Tech.*, 23:60–64, 1984.

[36] R. Krishna, Y.K. Kuchhal, G.S. Sarna, and I.D. Singh. Visbreaking studies on Aghajari long residue. *Fuel*, 67:379–383, 1988.

[37] H.H. Al-Soufi, Z.F. Savaya, H.K. Mohammed, and I.A. Al-Azawi. Thermal conversion (visbreaking) of heavy Iraqi residue. *Fuel*, 67:1714–1715, 1988.

[38] J. Singh, M.M. Kumar, A.M. Saxena, and S. Kumar. Reaction pathways and product yields in mild thermal cracking of vacuum residues: A multi-lump kinetic model. *Chem. Eng. J.*, 108:239–248, 2005.

[39] K.L Kataria, R.P. Kulkarni, A.B. Pandit, J.B. Joshi, and M. Kumar. Kinetic studies of low severity visbreaking. *Ind. Eng. Chem. Res.*, 43:1373–1387, 2004.

[40] W.R. Shu and L.L. Ross. Cracking severity index in pyrolysis of petroleum fractions. *Ind. Eng. Chem. Proc. Des. Dev.*, 21:371–377, 1982.

[41] C.E. Van Camp, P.S. Van Damme, P.A. Willems, P.J. Clymans, and G.F. Froment. Severity in the pyrolysis of petroleum fractions. fundamentals and industrial application. *Ind. Eng. Chem. Proc. Des. Dev.*, 24:561–570, 1985.

[42] T.Y. Yan. Characterization of visbreaker feeds. *Fuel*, 69:1062–1064, 1990.

[43] American Society of Testing and Materials. *Annual Book of ASTM Standards 2001, Section 5 Petroleum Products, Lubricants, and Fossil Fuels, Vol.05.06.* American Society of Testing and Materials, 2001.

[44] S. Peramanu, B.B. Pruden, and P. Rahimi. Molecular weight and specific gravity distributions for Athabasca and Cold Lake bitumens and their saturate, aromatic, resin, and asphaltene fractions. *Ind. Eng. Chem. Res.*, 38:3121–3130, 1999.

[45] S. Japanwala, K.H. Chung, H.D. Dettman, Gray, and M.R. Quality of distillates from repeated recycle of residue. *Energy and Fuels*, 16:477–484, 2002.

[46] C.M. Smith and P.E. Savage. Reactions of polycyclic alkylaromatics. 4. hydrogenolysis mechanisms in 1-alkylpyrene pyrolysis. *Energy and Fuels*, 6:195–202, 1992.

[47] S. Ratz, P.E. Savage, and L. Tan. Pyrolysis kinetics for long-chain n-alkylcyclohexanes. *Ind. Eng. Chem. Res.*, 40:1805–1810, 2001.

[48] J.P. Holman. *Experimental Methods for Engineers, 3rd Edition*. McGraw-Hill, 1978.

Appendix A

List of Carbon Types from Nuclear Magnetic Resonance

A.1 Carbon Types from NMR Spectroscopy

The major carbon types obtained from NMR spectroscopy and their relative amounts in the feed are shown in Table A.1. The additional carbon types within each major carbon types and their relative amounts in the feed are listed after Table A.1.

Table A.1: Major Carbon Types from NMR Spectroscopy

Carbon Type	Mole Fraction
Aromatic	0.2979
Cycloparaffinic	0.3153
Branched Paraffin	0.0746
Paraffin Chain ($> C_2$)	0.0995
Olefin	0.0041
Ring M & E & DPM	0.0952
Chain Attachments (α,β)	0.1133

In Table A.1, the M, E, and DPM stand for methyl, ethyl, and diphenylmethane. The aromatic and olefinic carbon types are listed in Table A.2.

In Table A.2, Aromatic NS stands for aromatic nitrogen and sulfur, respectively. The additional cycloparaffin and paraffin carbon types are listed in Table A.3.

Table A.2: Aromatic & Olefinic Carbon Types

Carbon Type	Mole Fraction
Aromatic NS (C + CH)	0.0364
Aromatic Bridge C	0.0619
Aromatic Alkyl Subst. C	0.0965
Aromatic CH	0.1032
Methyl-Aromatic	0.0183
Ethyl-Aromatic	0.0163
Propyl-Aromatic	0.0078
Diphenylmethane CH_2	0.0118
Olefin CH	0.0031
Olefin CH_2	0.0002
Olefin $CH_2(=C)$	0.0007

Table A.3: Cycloparaffinic & Paraffinic Carbon Types

Carbon Type	Mole Fraction
Cycloparaffin Bridge CH	0.0326
Cycloparaffin Alkyl Subst. CH	0.0821
Cycloparaffin CH_2	0.1999
Cycloparaffin $C(=CH_2)$	0.07
Methyl-Cycloparaffin	0.0215
Ethyl-Cycloparaffin	0.0273
Paraffin Chain	0.0917

The branched-paraffin carbon types are listed in Table A.4.

Table A.4: Branched-Paraffinic Carbon Types

Carbon Type	Mole Fraction
Methyl-Branched Chain	0.0693
Ethyl-Branched Chain	0.0041
+Butyl-Branched Chain	0.0012

Finally, the chain attachment carbon types are listed in Table A.5.

Table A.5: Chain Attachment Carbon Types

Carbon Type	Mole Fraction
α to Sulfides	0.0130
$\alpha\beta$ to Aromatic Rings	0.0346
α to Olefin	0.0031
α to Cycloparaffin Rings	0.0469
$\alpha\beta$ to Branch Points	0.0156

Appendix B

List of Product Gases

B.1 Product Gases

For the model, the product gases were grouped into methane, C_2, C_3+, and H_2S. A complete list of the product gases and their amounts from Run 2 is listed in Table B.1.

Table B.1: Complete List of Product Gases

Gas	Moles	Gas	Moles
Hydrogen (H_2)	0.148	1-Butene (C_4H_8)	0.008
Methane (CH_4)	0.484	iso-Butene (i-C_4H_8)	0.018
Ethylene (C_2H_4)	0.009	cis-2-Butene (C_4H_8)	0.003
Ethane (C_2H_6)	0.205	iso-Pentane (i-C_5H_{12})	0.012
Hydrogen Sulfide (H_2S)	0.461	3-Methyl-1-Butene (C_5H_{10})	0.001
Propane (C_3H_8)	0.147	trans-2-Pentene (C_5H_{10})	0.003
Propylene (C_3H_6)	0.030	1-Pentene (C_5H_{10})	0.003
iso-Butane (i-C_4H_{10})	0.014	2-Methyl-1-Butene (C_5H_{10})	0.002
n-Butane (n-C_4H_{10})	0.052	cis-2-Pentene (C_5H_{10})	0.003
trans-2-butene	0.005	Hexanes+ (C_6H_{14})	0.0029

Appendix C

Severity Index Correlation Plots

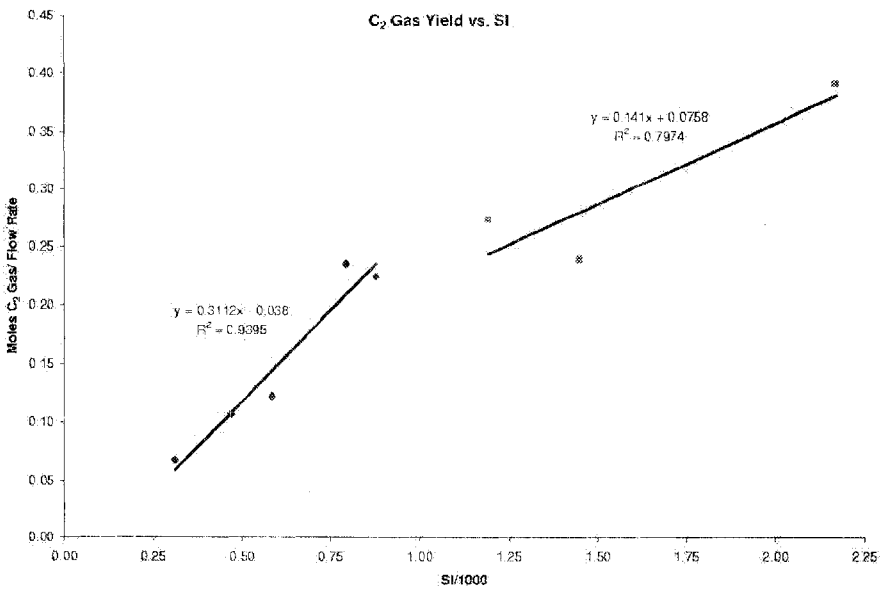

Figure C.1: Correlation of C_2 Gas Yield with Severity Index

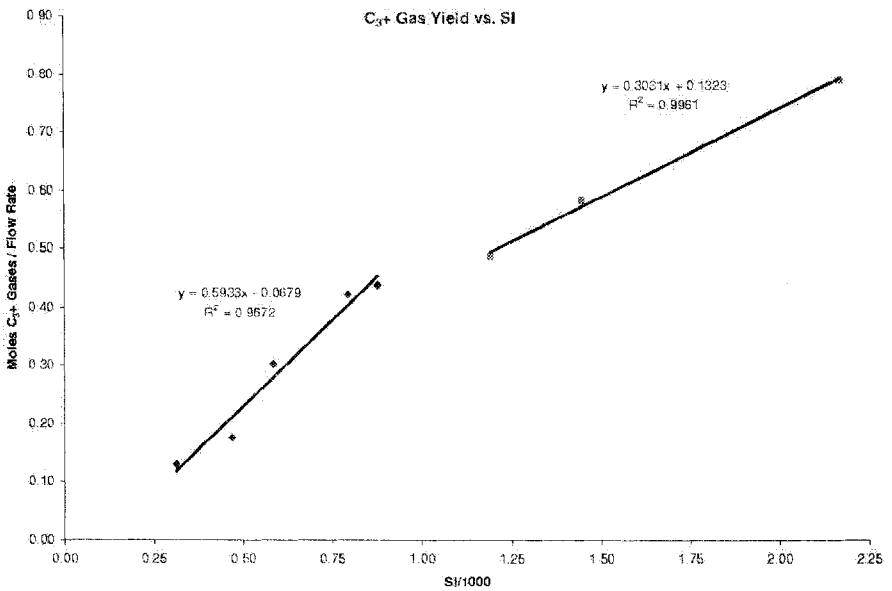

Figure C.2: Correlation of C_3+ Gas Yield with Severity Index

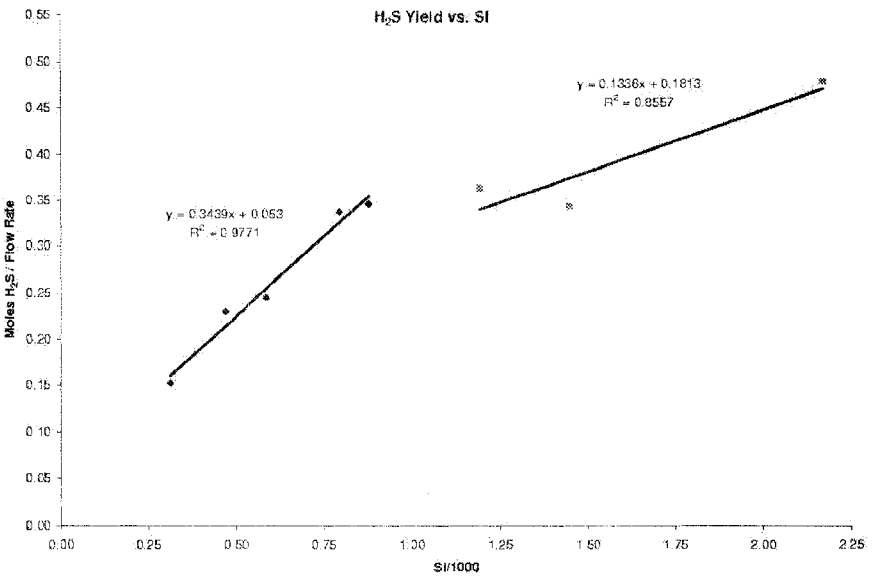

Figure C.3: Correlation of H_2S Gas Yield with Severity Index

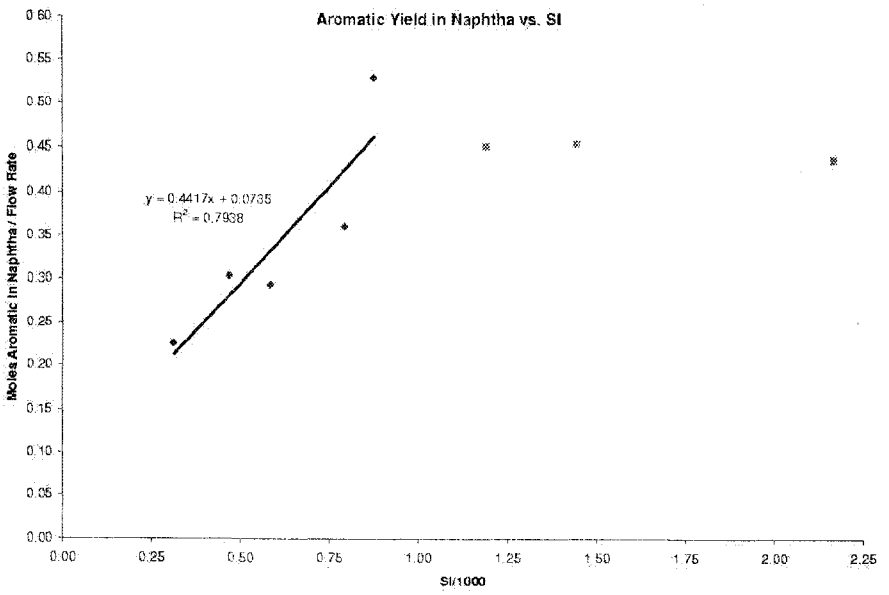

Figure C.4: Correlation of Naphtha Aromatic Yield with Severity Index

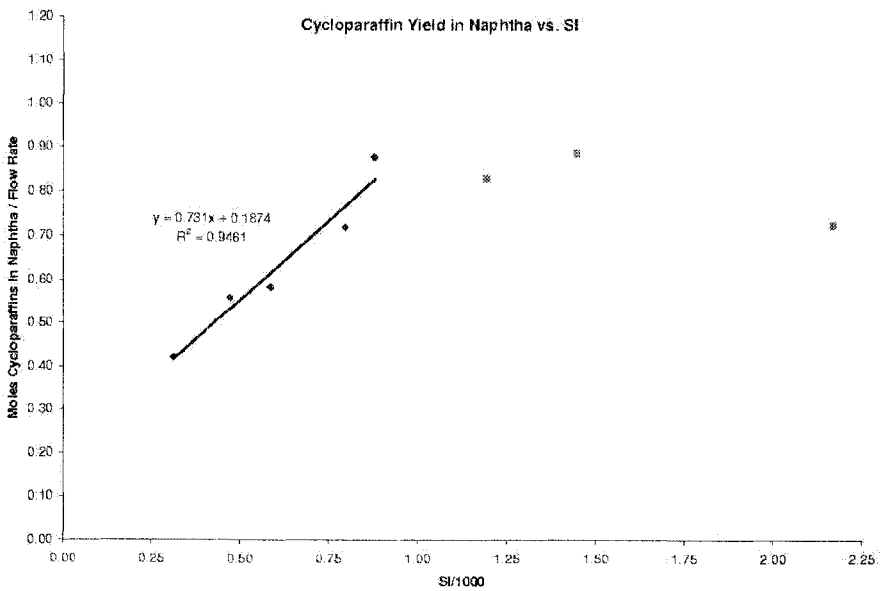

Figure C.5: Correlation of Naphtha Cycloparaffinic Yield with Severity Index

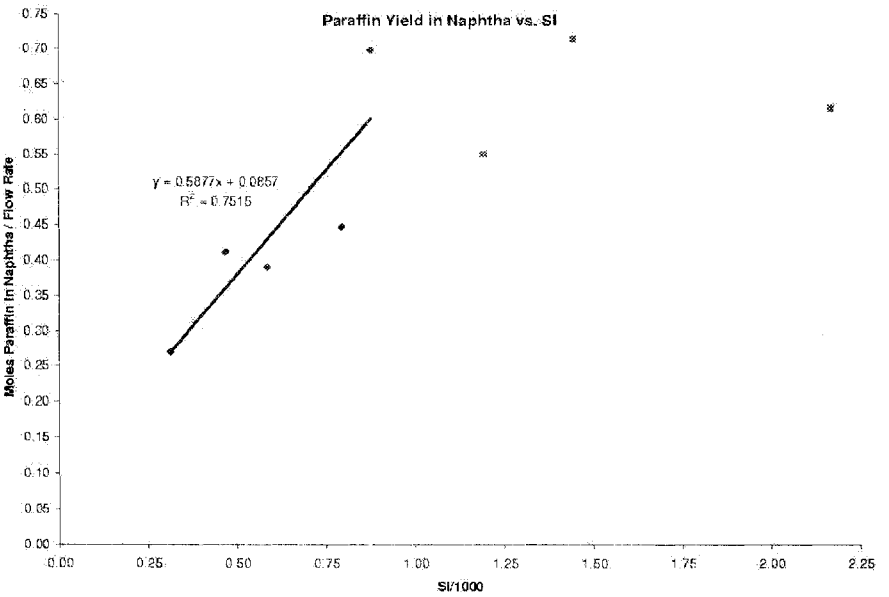

Figure C.6: Correlation of Naphtha Paraffinic Yield with Severity Index

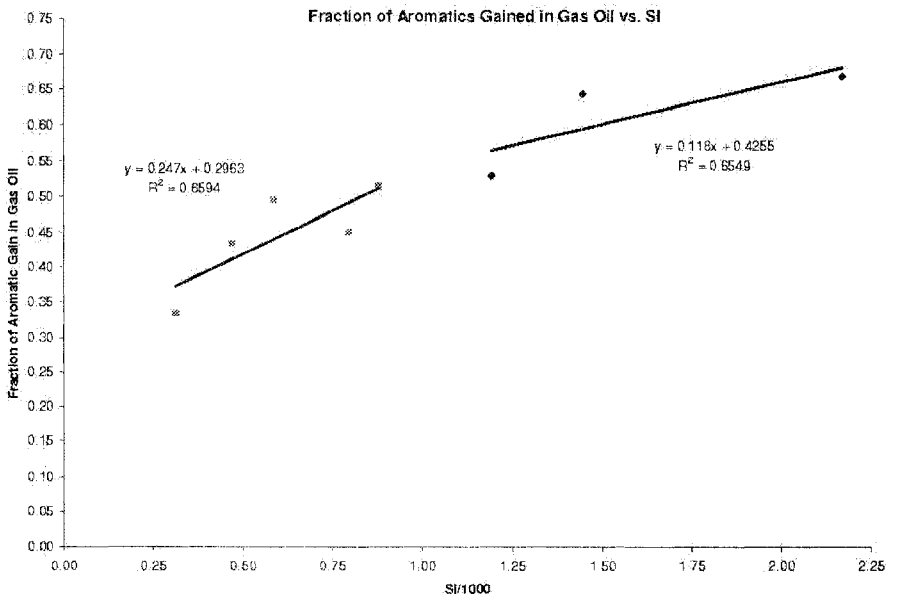

Figure C.7: Correlation of Gas Oil Aromatic Yield with Severity Index

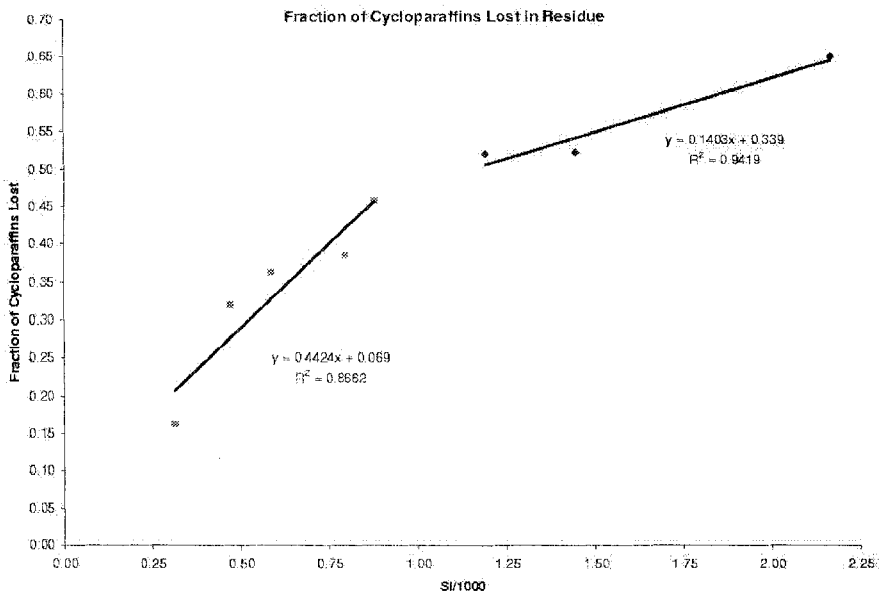

Figure C.8: Correlation of Residue Cycloparaffinic Yield with Severity Index

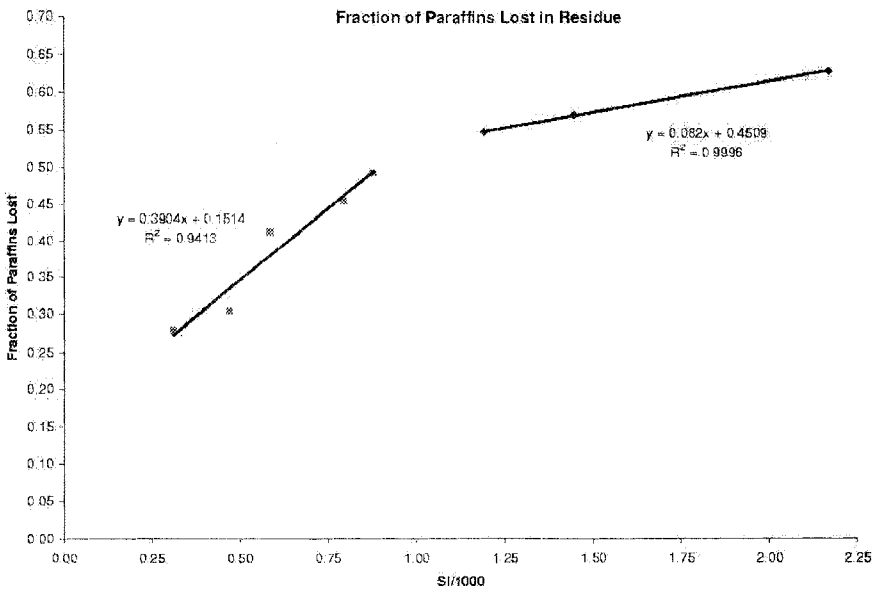

Figure C.9: Correlation of Residue Paraffinic Yield with Severity Index

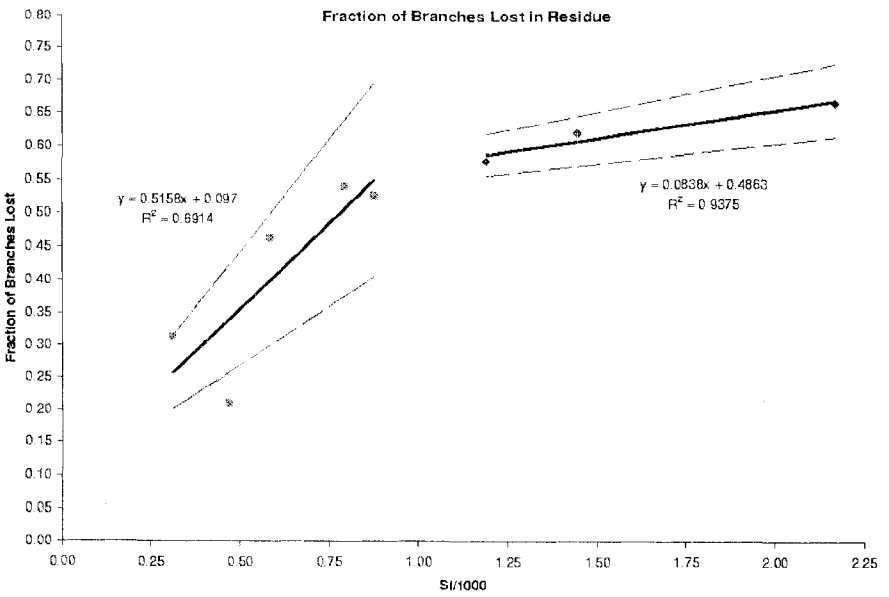

Figure C.10: Correlation of Residue Branch-Paraffinic Yield with Severity Index

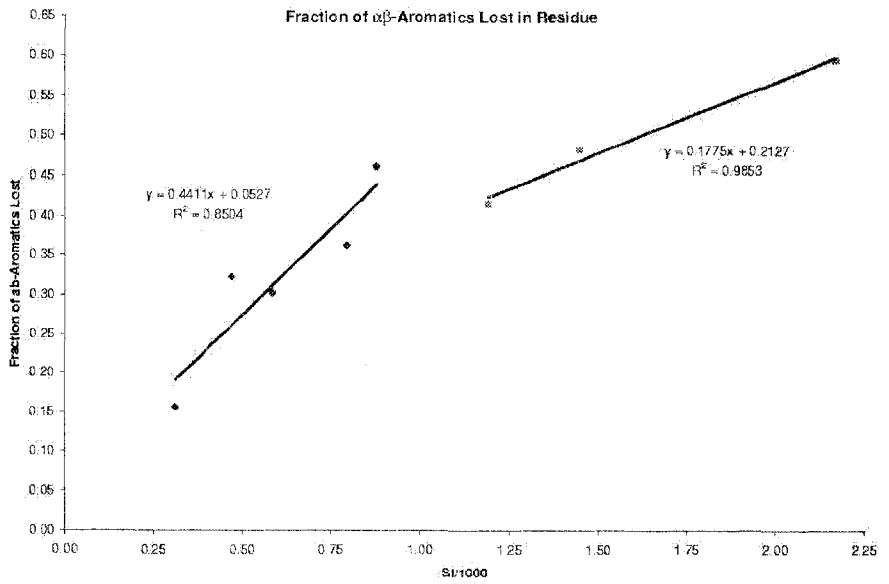

Figure C.11: Correlation of Residue $\alpha\beta$ to Aromatic Yield with Severity Index

Appendix D

Sample Calculations

The following is a complete set of sample calculations for model development and usage. Suppose a hypothetical set of visbreaking conditions was given where: T = 410^{o}C, residence time = 25 min, Feed = 2 kg/h. The following is a demonstration of the calculations performed to predict the product compositions and yields at these conditions.

D.1 Model Development

Step 1 Calculation of Severity Index and Reduced Severity For the given set of experimental conditions, the first step is to calculate severity index. The activation energy used was 242.7 kJ/mol. Substituting the conditions into the severity index equation:

$$SI = (1500) * exp\left(-\frac{242700}{8.314}\left(\frac{1}{683.15} - \frac{1}{700}\right)\right) \quad \text{(D.1)}$$

$$SI = 536.3\text{seconds} \quad \text{(D.2)}$$

To obtain the reduced severity, simply divide the severity index by 1000 to get 0.5363.

Step 2 Calculate Mass of Each Distillate Fraction. To obtain the overall gas, naphtha, and residue fraction yields, the lower severity correlations are used be-

cause the reduced severity is less than 1. The gas oil fraction yield is obtained by difference from the yields of the other fractions. Once the yields are obtained, multiply by the feed flow rate (2 kg/h = 2000 g/h) to obtain the mass.

- Gas: 0.0684 * 0.5363 - 0.0032 = 0.0335

  2000 * 0.0335 = 67 grams
- Naphtha: 0.0409 * 0.5363 + 0.0102 = 0.0321

  2000 * 0.0321 = 64.2 grams
- Residue: -0.1381 * 0.5363 + 0.4976 = 0.4235

  2000 * 0.4235 = 847.1 grams
- Gas Oil: 1 - 0.0335 - 0.0321 - 0.4235 = 0.5109

  2000 * 0.5109 = 1021.8 grams

Step 3 Calculate the Moles of the Gas Products The individual gas product yields obtained from the correlations are normalized yields so they have to multiplied by the feed flow rate (2 kg/h) to obtain the actual yield.

- Methane: 0.6385 * 0.5363 - 0.0624 = 0.2800

  2 * 0.2800 = 0.560 moles
- C_2: 0.3112 * 0.5363 - 0.0380 = 0.1289

  2 * 0.1289 = 0.258 moles
- C_3+: 0.5933 * 0.5363 - 0.0679 = 0.2503

  2 * 0.2503 = 0.501 moles
- H_2S: 0.3439 * 0.5363 - 0.0530 = 0.1314

  2 * 0.1314 = 0.263 moles

Step 4 Calculate the Yields of Naphtha Carbon Types Like the gases, the yields of the naphtha cycloparaffin, paraffin, and aromatic carbon types are normalized.

- Cycloparaffin: 0.7310 * 0.5363 + 0.1874 = 0.5794

  2 * 0.5794 = 1.159 moles
- Paraffin: 0.5877 * 0.5363 + 0.0857 = 0.4009

  2 * 0.4009 = 0.802 moles
- Aromatic: 0.4417 * 0.5363 + 0.0735 = 0.3104

  2 * 0.3104 = 0.621 moles

Step 5 Calculate the Yields of Gas Oil Carbon Types Cycloparaffin carbon yield did not show a strong trend so an average value of 0.1521 was taken. For the cycloparaffin, aromatic, and chain midsection carbon, the feed carbon data is required.

- Cycloparaffin: 24.39 * (1 - 0.1521) = 20.68 moles
- Aromatic: 15.16 * (1 + (0.247 * 0.5363 + 0.2963)) = 21.66 moles
- Chain Mids: 1.36 * (1 + (0.5425 * 0.5363 + 0.5936)) = 2.56 moles

Step 6 Calculate the Yields of Residue Carbon Types Aromatic carbon yield did not show a strong trend so an average value of 0.0356 was taken. Like the gas oil, the feed carbon data is required to estimate carbon type yields.

- Cycloparaffin: 20.35 * (1 - (0.4424 * 0.5363 + 0.069)) = 14.12 moles
- Aromatic: 26.53 * (1 - 0.0356) = 25.58 moles
- Paraffin: 9.99 * (1 - (0.3924 * 0.5363 + 0.1514)) = 6.38 moles
- Branch-Paraffin: 3.76 * (1 - (0.5158 * 0.5363 + 0.097)) = 2.36 moles

- Chain Mids: 6.46 * (1 - (0.3271 * 0.5363 + 0.1788)) = 4.17 moles
- α/β-Aromatic: 3.01 * (1 - (0.4411 * 0.5363 + 0.0527)) = 2.14 moles

Step 7 Coke Yield Because the reduced severity is less than 1, the predicted coke yield is taken to be 0.58 wt%.

Thus, for the hypothetical set of visbreaking conditions, Table D.1 lists the distillate fraction and carbon type yields.

Table D.1: Hypothetical Visbreaking Yields

Yield	Amount
Gas Fraction	67 grams
Naphtha Fraction	64.2 grams
Gas Oil Fraction	847.1 grams
Residue Fraction	1021.8 grams
Methane	0.560 moles
C_2	0.258 moles
C_3+	0.501 moles
H_2S	0.263 moles
Gas Oil Cycloparaffins	20.68 moles
Gas Oil Aromatics	21.66 moles
Gas Oil Chain Mids	2.56 moles
Residue Cycloparaffins	14.12 moles
Residue Aromatics	25.58 moles
Residue Paraffins	6.38 moles
Residue Branch-Paraffins	2.36 moles
Residue Chain Mids	4.17 moles
Residue α/β-Aromatic	2.14 moles

D.2 Error Calculations

D.2.1 Percent Difference

An example of the percent difference calculation (equation 5.4) is shown here. The data from Run 7 for the conservation of methyl species will be used for all

difference calculations. As a reminder, the equation is

$$\text{Difference} = 2\left\|\frac{Feed - Product}{Feed + Product}\right\| \tag{D.3}$$

For Run 7 in Table 5.1, the moles of feed methyl species is 3.32 and the moles of product methyl species and methane is 3.45.

Substituting the numbers for the feed and product into equation D.3,

$$\text{Difference} = 2\left\|\frac{3.32 - 3.45}{3.32 + 3.45}\right\| = -0.038 \tag{D.4}$$

Converting the result into a percentage gives a difference of -3.8%. All of the percent differences were calculated this way.

There were two different types of error analyses performed for the severity index correlations. Examples of both are shown here.

Example 1 Prediction Error

The equation to calculate the error bounds on the correlation equations is

$$\frac{\partial y}{\partial SI} = \frac{dy}{dSI}\Delta SI \tag{D.5}$$

$$\Delta SI = \sqrt{\left(\frac{\partial SI}{\partial E_A}\Delta E_A\right)^2 + \left(\frac{\partial SI}{\partial \tau}\Delta\tau\right)^2 + \left(\frac{\partial SI}{\partial T}\Delta T\right)^2} \tag{D.6}$$

where ΔE_A = 5000 cal/mol, $\Delta\tau$ = 2 min (120 seconds), and ΔT = 5 K. For equation D.5, $\frac{dy}{dSI}$ is the derivative of the correlation with respect to SI. Since the correlations are all linear, the derivative is simply the slope of the correlation.

Equation D.6 requires the partial derivatives of the original severity index equation with respect to activation energy, residence time, and temperature. This method is known as the Holman method [48].

$$\frac{\partial SI}{\partial \tau} = exp\left(-\frac{E_A}{R}\left(\frac{1}{T} - \frac{1}{700}\right)\right) \tag{D.7}$$

$$\frac{\partial SI}{\partial E_A} = \frac{-\tau}{R}\left(\frac{1}{T} - \frac{1}{700}\right) exp\left(-\frac{E_A}{R}\left(\frac{1}{T} - \frac{1}{700}\right)\right) = \frac{-SI}{R}\left(\frac{1}{T} - \frac{1}{700}\right) \tag{D.8}$$

$$\frac{\partial SI}{\partial T} = \frac{\tau E_A}{RT^2} exp\left(-\frac{E_A}{R}\left(\frac{1}{T} - \frac{1}{700}\right)\right) = \frac{SIE_A}{RT^2} \tag{D.9}$$

In the 3 partial derivative equations above, the SI is the original severity index and not reduced severity. However, when doing the error calculations, reduced severity is used because that was the quantity plotted on the x-axis.

In this example, the calculations for the error bounds for the overall naphtha yield correlation from Figure 5.3 will be shown. From Table 4.1, the severity index for Run 7 was 585.2 and the reduced severity was 0.5852. The correlation for the overall naphtha yield in the low severity region is:

$$y = 0.0409SI + 0.0102 \tag{D.10}$$

Substituting the proper numbers into equation D.5 and the 3 partial derivative equations:

$$\frac{dy}{dSI} = 0.0409 \tag{D.11}$$

$$\frac{\partial SI}{\partial \tau} = exp\left(-\frac{58000}{1.987}\left(\frac{1}{688.15} - \frac{1}{700}\right)\right) = 0.4877 \tag{D.12}$$

$$\frac{\partial SI}{\partial E_A} = \frac{-585.2}{1.987}\left(\frac{1}{688.15} - \frac{1}{700}\right) = -0.00725 \tag{D.13}$$

$$\frac{\partial SI}{\partial T} = \frac{(585.2)(58000)}{(1.987)(688.15)^2} = 36.0718 \tag{D.14}$$

Now, substituting these numbers into equation D.6,

$$\Delta SI = \sqrt{(0.4877 * 120)^2 + (-0.00725 * 5000)^2 + (36.0718 * 5)^2} = 193.05 \tag{D.15}$$

$$\frac{\partial y}{\partial SI} = 0.0409 * 193.05 = 7.896 \tag{D.16}$$

Finally, the value of $\frac{\partial y}{\partial SI}$ is divided by 1000 to make it the error for the reduced severity and in this case, it is 0.007896. Thus, for when predicting the overall naphtha fraction yield at a reduced severity of 0.5852, the predicted yield would be

$$y = 0.0341 \pm 0.008. \tag{D.17}$$

Example 2 Measurement Error

The quantities plotted on the y-axis of the correlation plots have one of two forms:

$$y = \frac{a}{b} \tag{D.18}$$

$$y = 1 - \frac{b}{a} \tag{D.19}$$

A similar approach using partial derivatives is used here as well.

$$Error = \sqrt{\left(\frac{\Delta a}{b}\right)^2 + \left(\frac{a}{b^2}\Delta b\right)^2} \tag{D.20}$$

$$Error = \sqrt{\left(\frac{b}{a^2}\Delta a\right)^2 + \left(\frac{\Delta b}{a}\right)^2} \tag{D.21}$$

Here, the error calculations for the methane yield in Run 7 will be shown. In Run 7, from Table 4.5, 0.771 moles of methane were formed. On the plot of the correlation of methane yield with severity index (Figure 5.2), the quantity plotted on the y-axis is moles of methane formed per kg/h of feed so equations D.18 and D.20 apply. From Table 6.2, a = moles of Methane formed and b = feed flow rate in equation D.18. The error for the methane and feed flow rate measurements was taken as 10%. Substituting the numbers into equation D.20 gives

$$Error = \sqrt{\left(\frac{0.1 * 0.771}{3}\right)^2 + \left(\frac{(0.1)(3)0.771}{3^2}\right)^2} = 0.0363 \tag{D.22}$$

Thus, the data point for methane yield in Run 7 would be 0.257 ± 0.036 moles per kg/h of feed.